

RESEARCH

Open Access



WIF-1 contributes to lupus-induced neuropsychological deficits via the CRYAB/STAT4-SHH axis

Liping Tan^{1,2}, Yu Fan^{1,2}, Xinyi Xu³, Tianshu Zhang^{1,2}, Xiangyu Cao^{1,2}, Chenghao Zhang^{1,2}, Jun Liang^{3*}, Yayi Hou^{1,2*} and Huan Dou^{1,2*}

Abstract

Background Neuropsychiatric systemic lupus erythematosus (NPSLE) often manifests as cognitive deterioration, with activated microglia and blood-brain barrier (BBB) disruption implicated in these neurological complications. Wnt-inhibitory factor-1 (WIF-1), a secreted protein, has been detected in the cerebrospinal fluid (CSF) of NPSLE patients. However, the contribution of WIF-1 in contributing to lupus cognitive impairment remains poorly understood.

Methods Using MRL/MpJ-Faslpr (MRL/lpr) lupus-prone mice and TLR7 agonist imiquimod (IMQ)-induced lupus mice, recombinant WIF-1 protein (rWIF-1) and adeno-associated virus (AAV) encoding sh-WIF-1 were administered via intracerebroventricular injection. Behavioral tests, histopathological examinations, flow cytometry, and molecular biology techniques were employed to investigate the underlying mechanisms.

Results Microinjection of rWIF-1 exacerbated cognitive deficits and mood abnormalities, increased BBB leakage and neuronal degeneration, and caused aberrant activation of microglia and synaptic pruning in the hippocampus. Conversely, lupus mice injected with AAV-shWIF-1 exhibited significant remission. In vitro, rWIF-1 induced overactivation of microglia with an increased CD86⁺ pro-inflammatory subpopulation, upregulated phagocytic activity, and excessive synaptic engulfment, contributing to increased BBB permeability. Furthermore, WIF-1 exerted its biological effects through the CRYAB/STAT4 pathway, transcriptionally decreasing SHH production. We also identified that symmetric dimethylarginine (SDMA) could alleviate rWIF-1-induced microglial activation and BBB damage, thereby restoring SHH levels.

Conclusions In conclusion, WIF-1 exacerbates lupus-induced cognitive dysfunction in mice by triggering aberrant microglial activation and BBB disruption through the CRYAB/STAT4-SHH axis, highlighting the potential therapeutic effects of SDMA for the treatment of NPSLE.

Keywords Neuropsychiatric systemic lupus erythematosus, WIF-1, Microglia, Blood-brain barrier

*Correspondence:

Jun Liang
13505193169@139.com
Yayi Hou
yayihou@nju.edu.cn
Huan Dou
douhuan@nju.edu.cn

¹The State Key Laboratory of Pharmaceutical Biotechnology, Division of Immunology, Medical School, Nanjing University, Nanjing 210093, China
²Jiangsu Key Laboratory of Molecular Medicine, Nanjing 210093, China
³Department of Rheumatology and Immunology, Nanjing Drum Tower Hospital, The Affiliated Hospital of Nanjing University Medical School, Nanjing 210008, China



© The Author(s) 2024. **Open Access** This article is licensed under a Creative Commons Attribution-NonCommercial-NoDerivatives 4.0 International License, which permits any non-commercial use, sharing, distribution and reproduction in any medium or format, as long as you give appropriate credit to the original author(s) and the source, provide a link to the Creative Commons licence, and indicate if you modified the licensed material. You do not have permission under this licence to share adapted material derived from this article or parts of it. The images or other third party material in this article are included in the article's Creative Commons licence, unless indicated otherwise in a credit line to the material. If material is not included in the article's Creative Commons licence and your intended use is not permitted by statutory regulation or exceeds the permitted use, you will need to obtain permission directly from the copyright holder. To view a copy of this licence, visit <http://creativecommons.org/licenses/by-nc-nd/4.0/>.

Introduction

Neuropsychiatric systemic lupus erythematosus (NPSLE) is a severe central nervous system involvement of systemic lupus erythematosus (SLE) [1], and stands as the second leading cause of death among lupus patients [2]. In 1999, the American College of Rheumatology (ACR) elucidated nineteen distinct neuropsychiatric syndromes attributable to SLE, which can be subdivided into focal (e.g., stroke, movement disorders) and diffuse (e.g., anxiety disorder, cognitive dysfunction) symptoms [3]. Subsequently, Ainala et al. revised the initial clinical diagnostic classification in 2001 [4]. According to published estimates, up to 95% of SLE patients experience these manifestations heterogeneously [5, 6]. Multiple studies have consistently demonstrated that cognitive deficits, including mood and anxiety disorders, learning, and memory impairment, are the most frequent NPSLE symptoms, often presenting in patients with an inflammatory phenotype [6, 7]. These symptoms are insidious and typically develop slowly over time, independent of disease activity [8]. However, the limited understanding of pathophysiological mechanisms has hindered the discovery of specific biomarkers, which are essential for the gold standard of NPSLE diagnosis [9].

The blood-brain barrier (BBB) serves as a protective shield that safeguards the central nervous system against the infiltration of detrimental external substances. Endothelial tight junctions and specific transcellular/efflux transport systems form the primary barrier against toxins, pathogens, peripheral inflammation, and immune cells. During the pathological process, BBB function deteriorates contributing to cognitive impairment and neurologic disorders [10–12]. An association has been reported between extensive BBB leakage and cognitive impairment in SLE patients [13]. We also observed that the intraperitoneal injection of a highly piperazine-derived compound, K-7174, improved cognitive dysfunction in lupus-prone mice by directly acting on brain microvascular endothelial cells and reducing the permeability of the BBB [14]. Microglia, along with endothelial cells, pericytes, astrocytes, and neuroblasts, constitute the fundamental unit of the BBB, known as the neurovascular unit, which regulates and maintains barrier function [15, 16]. The activation and subsequent coordination of microglia play an early role in various neurodegenerative disease-related BBB damage [17–20]. Their ablation can adversely influence BBB integrity via the release of cytokines, reactive oxygen species, or matrix metalloproteinases (MMPs) [21]. In lupus-prone mice (NZB/NZW, MRL/lpr, and FcγRIIB^{-/-}Yaa), microglial cells abnormally activate in the hippocampal area, exhibiting a spectrum of pathogenetic properties including increased release of cytokines and chemokines, and enhanced antigen presentation, leading to worsening depression and cognitive

dysfunction [22–26]. Even in the early stage of NPSLE, microglia show abnormal activation, disrupting neuronal formation despite an intact BBB [26]. In conclusion, activation of microglia in NPSLE regulates BBB remodeling, and inhibition of microglia activation is of great significance to protect BBB integrity.

Beyond these effects, the drivers of aberrant behaviors, BBB disruption, and particularly, microglial phenotype in lupus progression remain unclear. In our previous studies, various omics techniques were employed to screen the comprehensive expression profile of lncRNAs, messenger RNAs (mRNAs), and proteins in NPSLE patients, active SLE patients who had never experienced neuropsychiatric manifestations (Non-NPSLE), and healthy controls [27–29]. We identified an abnormal level of the secreted protein Wnt-inhibitory-factor-1 (WIF-1) in the cerebrospinal fluid (CSF) of NPSLE patients. While WIF-1 expression is mainly present in the heart, lungs, eyes, and brain of adult mice, albeit at lower levels, it has been confirmed that WIF-1 directly contributes to myelination and hippocampal development [30, 31]. Aberrant expression of WIF-1 is strongly linked to cognitive deficits and an increased risk of dementia [32–34]. Additionally, Niu et al. found that the secretion of WIF-1 disrupts endothelial tight junction integrity, exacerbating BBB permeability and inducing central nervous system (CNS) inflammation [35]. Intriguingly, the downregulation of WIF-1 expression may potentially enhance the proliferation and adhesion capabilities of CD4⁺ T cells in patients with SLE, providing new insight as a diagnostic marker [36]. However, the underlying cellular and molecular mechanisms by which WIF-1 leads to NPSLE remain elusive.

This study aims to investigate the interplay between WIF-1 and the progression of NPSLE using TLR7 agonist imiquimod (IMQ)-induced and MRL/MpJ-Fas^{lpr} (MRL/lpr) spontaneous lupus-prone mouse models. Firstly, we assessed the effects of intraventricular injection of recombinant WIF-1 (rWIF-1) and AAV-shWIF-1 on the neurobehavioral phenotype and BBB function in vivo. To elucidate WIF-1-related BBB leakage, we assessed microglia activation, synapse engulfment, and co-culturing of brain endothelial cells. Here, we provide evidence that WIF-1 exacerbates the progression of NPSLE through the CRYAB/STAT4-SHH axis, which may provide a potential therapeutic strategy to combat lupus cerebritis-associated BBB leakage.

Materials and methods

Reagents

Recombinant WIF-1 protein (50984-M08H, Sino Biological Inc., Beijing, China); ChIP Kits (53009 & 53035, Active Motif, Shanghai, China). Western Blot or Immunofluorescence Antibodies: WIF-1 Protein Primary

Antibody (ab155101, Abcam, Cambridge, UK), ZO1 Protein Primary Antibody (21773-1-AP, Proteintech, Chicago, USA), Occludin Protein Primary Antibody (13409-1-AP, Proteintech), Albumin Protein Primary Antibody (16475-1-AP, Proteintech), SHH Protein Primary Antibody (R25772, Zen-Bioscience, Chengdu, China), STAT4 Protein Primary Antibody (6775, Cell Signaling Technology, Massachusetts, USA), PSD95 Protein Primary Antibody (20665-1-AP, Proteintech), SYN1 Protein Primary Antibody (340966, Zen-Bioscience), CRYAB Protein Primary Antibody (15808-1-AP, Proteintech), LAPM1 Protein Primary Antibody (516894, Zen-Bioscience, Chengdu, China), IBA-1 Protein Primary Antibody (382207, Zen-Bioscience, Chengdu, China). Primers were obtained from Nanjing Sipujin Biotechnology Co., Ltd.

Adeno-associated virus (AAV) construction

The construction of the adeno-associated virus (AAV) used in this study followed the protocol previously reported by Piras et al. (2016). Briefly, AAV9 carrying the U6 promoter driving the expression of shRNA targeting WIF-1 (AAV9-U6 promoter-shWIF-1, indicated as shWIF-1). The shWIF-1 was produced by Nanjing Zebrafish Biotech Co., Ltd. (gene silencing sequence: 5'-GCTAG AGTGCTCATAGGATTT-3'). In order to serve as a control, vectors encoding a scrambled nucleotides sequence were used (5'-CCTAAGGTTAAGTCGCCCTCG-3').

Animal models and treatment

Female MRL/lpr, MRL/mpj and C57BL/6 mice, aged 6 to 8 weeks, were obtained from Cavens Biotechnology Co., Ltd. (Nanjing, China) and housed in a specific pathogen-free facility with a relative humidity of $55 \pm 5\%$, room temperature of $22 \pm 2^\circ\text{C}$, and a 12-hour light/dark cycle. The animals were allowed free access to drinking water and were acclimatized to the housing conditions for at least one week. To establish the IMQ-induced lupus mouse model, thirty C57BL/6 female mice were randomly divided into the following three groups: CON+PBS ($n=10$), IMQ+PBS ($n=10$), and IMQ+rWIF-1 ($n=10$). As shown in Fig. 1A, the right ears of the mice in the IMQ+PBS and IMQ+rWIF-1 groups were topically treated with 1.25 mg of 5% IMQ cream (Keyi Pharmaceutical Co., Ltd., China) three times weekly from week 0 to 8, while the equivalent amount of petroleum jelly was applied to the CON+PBS group [37]. In week 4 and 8, the IMQ+rWIF-1 group received intraventricular injections of rWIF-1 as previously reported [38]. The CON+PBS and IMQ+PBS groups were treated with an equivalent volume of PBS. At week 8, mice were anesthetized with 2.0% isoflurane (vol/vol) in a 600 cc/min oxygen flow via inhalation, and then perfused with cold PBS. Brains were extracted, one half were stored in a hypothermic environment for RNA sequencing, western blot (WB), and

enzyme-linked immunosorbent assay (ELISA), and the other half were fixed in the paraformaldehyde (PFA), preparing for the paraffin section.

To establish the MRL/lpr lupus-prone mouse model, twenty-four MRL/lpr mice were randomly divided into two groups: MRL/lpr+Vector (MRL/lpr+AAV9-Vector, $n=12$) and MRL/lpr+shWIF-1 (MRL/lpr+AAV9-shWIF-1, $n=12$), with MRL/mpj mice treated with AAV9-vector serving as the MRL/mpj+Vector group ($n=12$). As shown in Fig. 2A, at 10 weeks of age, mice were anesthetized with 2.0% isoflurane (vol/vol) in 600 cc/min oxygen flow via inhalation, and then each mouse received an injection of 3 μL (5×10^9 vg) viruses. The intracerebroventricular (ICV) injection were performed perpendicular to the skull ($x=0.8$ mm, $y=0.2$ mm, $z=2$ mm) using a microprocessor-controlled mini-pump (World Precision Instruments, Sarasota, FL, USA), delivery was performed at a rate of 500 nL/min. After injection, the needle was left in place for 5 min prior to slowly retracting it from the ventricles. Afterward the mice were left underneath a warm light to recover their mobility [39]. The mice in the MRL/lpr+shWIF-1 group received intraventricular injections of shWIF-1 virus, while the MRL/lpr+Vector and MRL/mpj+Vector groups were treated with an equivalent volume of AAV9-vector. At 20 weeks of age, animal tissue samples were collected as described above.

Coat Score: As described in the literature [40], the cleanliness of the mouse coat is indicative of self-care behavior. A quantitative scale was used to assess the fur condition, evaluating seven different body regions: head, neck, back fur, tail, forelimbs, hindlimbs, and ventral fur. Clean and neat fur received a score of 0, intermediate status received a score of 1, and dirty or abnormal fur received a score of 2. The scores for each region were summed to obtain the total score for fur condition. Statistical analysis was performed on the average values of the results.

All animal experimental procedures were performed under Brazilian Federal Law 1.794/2008 for the scientific use of animals and approved by the Institutional Animal Care and Use Committee of the Affiliated Drum Tower Hospital of Nanjing University Medical School (2023AE01037).

Functional behavioral tests

Y-maze

Objective To evaluate spatial working memory by recording spontaneous alternations.

Maze Structure The Y-maze had arms labeled A, B, and C (35 cm, 10 cm, and 15 cm, respectively) with an angle of 120° between the arms. The Y-maze test was performed as described by Choi [41]. Procedure: Mice were allowed

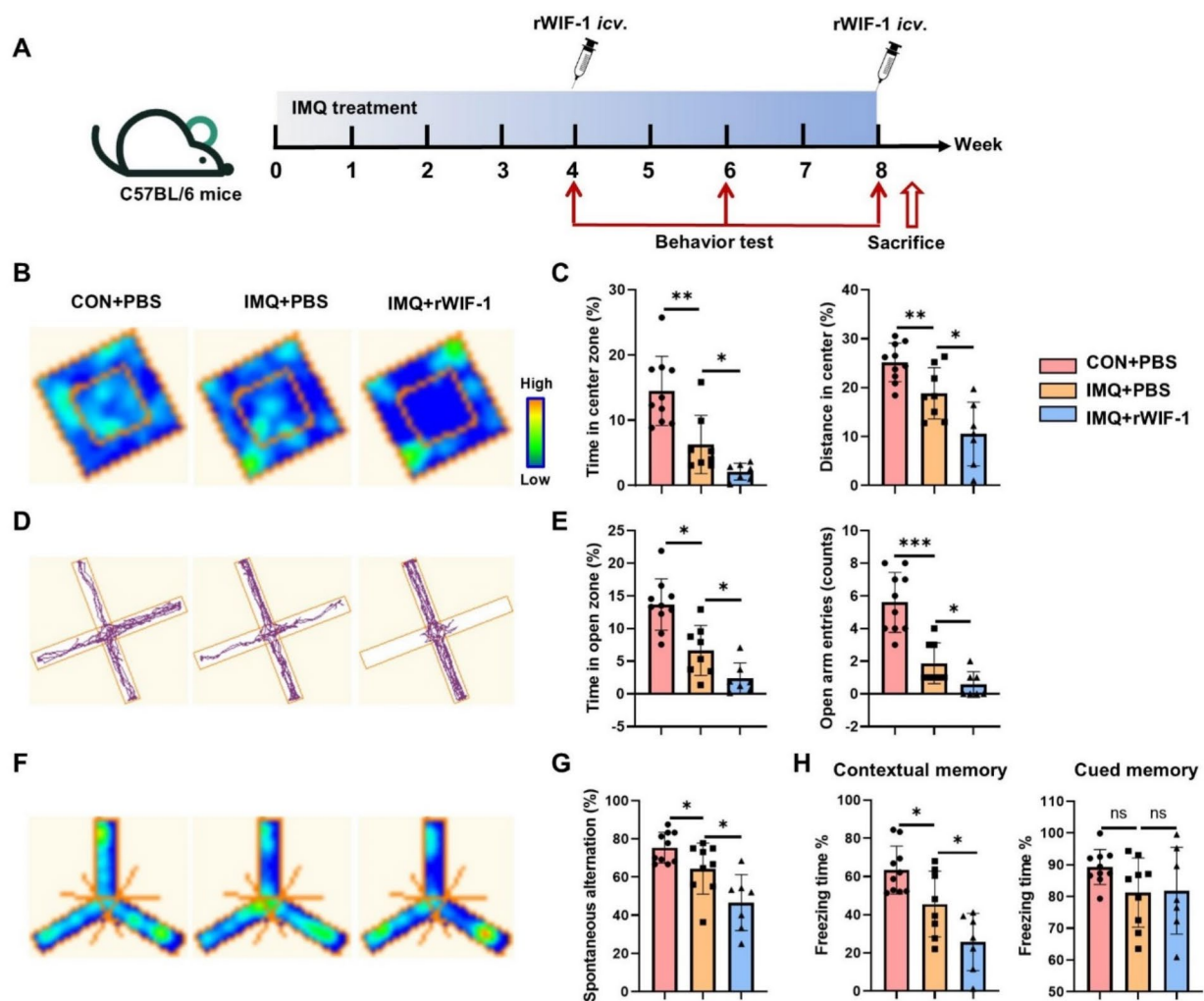


Fig. 1 Intracerebroventricular injection of rWIF-1 exacerbates abnormal behavior in IMQ mice. **(A)** Schematic representation of the IMQ mouse model, with WIF-1 administered via intracerebroventricular injection at weeks 4 and 8. The control group received PBS injections of the same volume. Behavioral tests were conducted on the day following each injection, with analysis performed at the conclusion of the final behavioral assessment. **(B, C)** Open Field Test (OFT) in the IMQ mouse model at week 8. **(D, E)** Elevated Plus Maze (EPM) test in the IMQ mouse model at week 8. **(G, J)** Y-maze test in the IMQ mouse model at week 8. **(H)** Contextual fear conditioning in the IMQ mouse model. *: $P < 0.05$; **: $P < 0.01$; ***: $P < 0.001$

to freely explore the maze for 8 min, and the AnyMaze system recorded arm entries. A successful alternation was defined as a non-repeated consecutive entry (e.g., ABC, BCA, CAB). The inside of the Y-maze was cleaned with 75% ethanol between trials and allowed to dry. Arm entry was defined as the entry of the whole body into an arm.

Calculation The percentage of spontaneous alternations = (Successful alternations / (number of total arm entries - 2)) × 100%.

Fear conditioning test

Objective Evaluate fear responses and assess the retention of contextual and cue memory in mice by recording freezing time.

Method Mice were individually placed into a dark chamber (25×25×25 cm) for fear conditioning tests, where the chamber floor was constructed of stainless steel rods connected to an electronic stimulator [42]. The experimental design comprised three phases: training, contextual memory testing, and cue memory testing. During the training phase, following a 3-minute exploration in the chamber, mice were exposed to a 100 dB, 4000 Hz sound stimulus for 30 s, culminating in a 0.8 mA electric shock delivered in the final 2 s.

For contextual memory testing, conducted 24 h after the previous day’s experiment, mice were placed in the same experimental chamber for 3 min without sound, and their freezing behavior was recorded. For cue memory testing, performed 2 h after contextual memory testing,

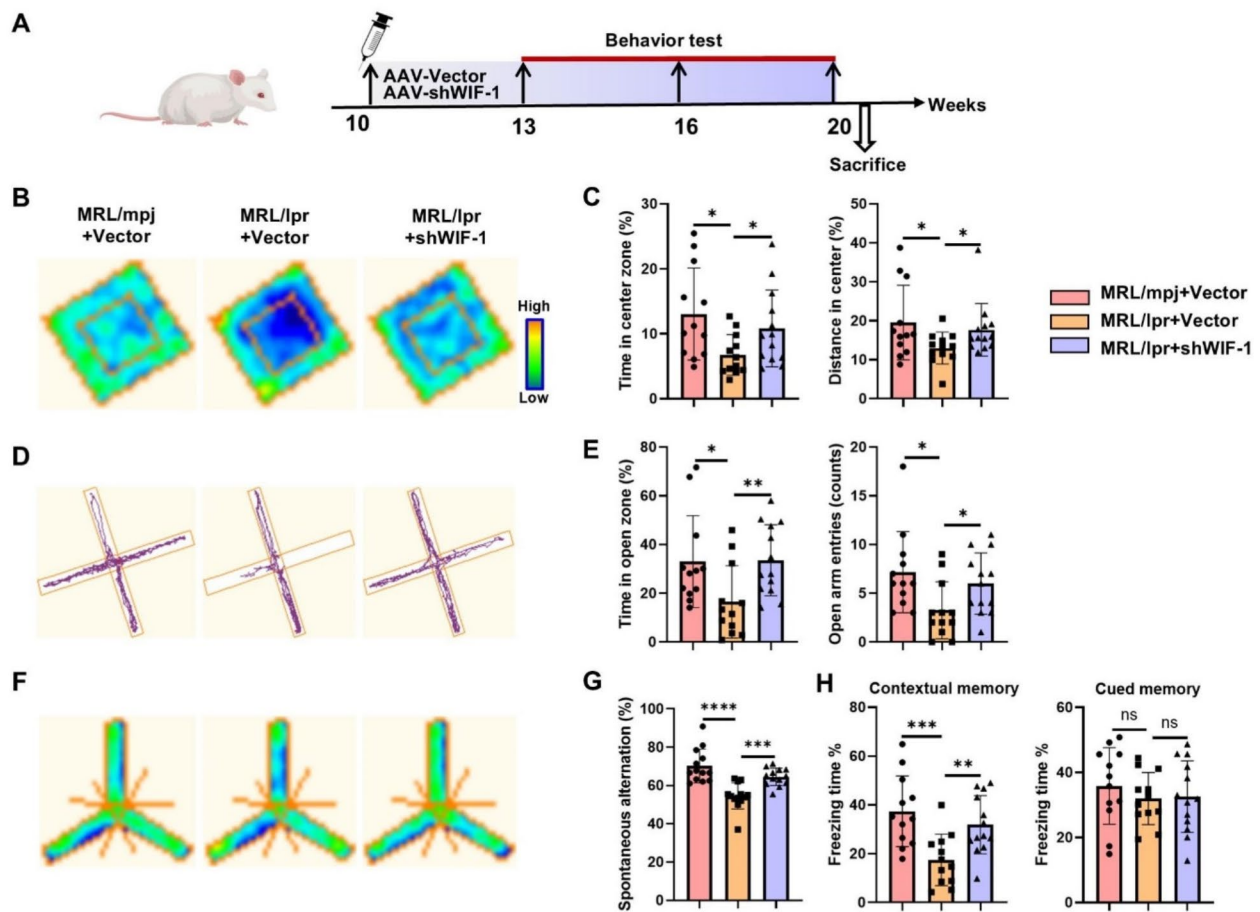


Fig. 2 Knockdown of WIF-1 in the brain using AAV alleviates abnormal behavior in MRL/lpr mice. **(A)** Schematic representation of the MRL/lpr mouse model, with AAV administered via intracerebroventricular injection at 9–10 weeks. Behavioral tests were conducted at 13, 16, and 20 weeks, with analysis performed at the conclusion of the final behavioral assessment. **(B, C)** OFT in the MRL/lpr mouse model at 20 weeks. **(D, E)** EPM test in the MRL/lpr mouse model at 20 weeks. **(F, G)** Y-maze test in the MRL/lpr mouse model at 20 weeks. **(H)** Contextual fear conditioning in the MRL/lpr mouse model at 20 weeks. *: $P < 0.05$; **: $P < 0.01$; ***: $P < 0.001$; ****: $P < 0.0001$

mice were placed in a different environment with altered board color and lighting for 3 min. Subsequently, they were exposed to the same sound stimulus for 30 s. The percentage of freezing time during sound presentation was recorded for each group.

Calculation Data were analyzed using Packwin 2.0 software.

Open field test (OFT)

Objective Evaluate anxiety and depression by recording distance in the centre and time in the centre zone.

Method As previously mentioned [43], the mice were placed alone in the centre of a 30 cm × 30 cm × 30 cm square open chamber for 30 s. Subsequently, the experimenter left the area, and the mice's activities in the central zone, total distance travelled, and average speed within

the open field were recorded using video cameras for a duration of 5 min. Following each trial, the testing apparatus was meticulously cleaned with 70% alcohol to eliminate potential olfactory interference from the preceding mouse, thereby ensuring unbiased subsequent trials. Throughout the experimental procedure, a quiet environment was maintained to minimize any stimuli that could impact the mice's behavior.

Calculation The different parameters measured, including total distance travelled in the whole arena, percentage of time spent in the centre of the arena, average velocity, and resting time, were analyzed using the associated software Any-maze (Stoelting Co., USA).

Elevated plus maze (EPM)

Objective Evaluate anxiety and depression by recording time in the open zone and counts in open arm entries.

Method In the same way as before [44], the animals were gently placed in the central zone of the apparatus, facing an open arm, after which the experimenter promptly and quietly withdrew. Subsequently, the trajectory movements of the animals within the elevated plus maze apparatus were monitored using the Any-maze system, with the experimental duration set at 5 min.

Calculation The percentage of time spent by the mice on the open arm and the frequency of entries into the open arm were calculated and analyzed.

Flow cytometry analysis

For mouse brain microglial cell detection, established methods as described in previous literature [39] were followed. In brief, mouse hippocampal/medial prefrontal cortex (mPFC) tissues were homogenized, filtered through a 70 μm cell strainer, and sorted by myelin removal beads. The cell suspension was then incubated with antibody dilutions (CD11b-PE CF594, CD45-PerCP, CD86-PE Cy7, LAMP1-PE), and washed twice with PBS for subsequent evaluation.

For the phagocytosis assay, cells were first starved with DMEM containing 1% serum for 24 h, then mixed with 0.1 $\mu\text{g}/\text{ml}$ pHrodo™Green Zymosan Bioparticles (Q-0056648, Thermo Scientific) and complete medium (5% serum). BV2 mouse microglia were treated for 2 h at 37 °C. The medium was discarded, and the cells were collected for later examination. Finally, all cell samples were analyzed using flow cytometry (Cytex Aurora, Cytex Biosciences, USA), and data were processed with FlowJo software (BD Biosciences). The t-distributed stochastic neighbor embedding (tSNE) was set with Barnes-Hut gradient algorithm, iteration of 1000, perplexity of 30, learning rate of 847 by flowjo plugin tSNE.

Cell culture and RNA sequencing (RNA-seq)

Mouse brain microvascular endothelial cell line (bEnd.3), mouse neuronal cell line (HT22), and mouse microglia cell line (BV2) were respectively cultured in DMEM containing 10% fetal bovine serum at 37 °C with 5% carbon dioxide. Cells were passaged every 2 to 3 days at 80% confluency. For RNA-seq analysis, BV2 cells were treated with or without rWIF-1 (1 $\mu\text{g}/\text{ml}$) for 24 h. The number of biological replicates was 3 for each condition. Total RNA was extracted using Trizol Reagent (Invitrogen, Life Technologies Corporation) according to the manufacturer's instructions. RNA quantity and purity were assessed with a Nanodrop 2000 spectrophotometer (Thermo Scientific). Transcriptome libraries were generated using the TruSeq™ RNA sample preparation Kit (Illumina, San Diego, CA) with 5 μg of total RNA. The library size was selected on 2% Low Range Ultra Agarose followed by PCR amplification using Phusion DNA polymerase

for 15 PCR cycles. Paired-end sequencing was performed on the HiSeq 2500 Platform (NovelBio Corp. Laboratory, Shanghai). The raw paired-end reads were trimmed and quality-controlled by SeqPrep and Sickle with default parameters. Clean reads were separately aligned to the reference genome using the orientation mode of TopHat (version 2.0.10) software [45]. To identify differentially expressed genes (DEGs) between two groups, the expression level of each transcript was calculated according to the fragments per kilobase of exon per million mapped reads (FPKM) method, using Cufflinks (version 2.1.1) [46]. The criteria for differential expression were a log₂ fold-change of >0.58 or <-0.58 and a Q value <0.05.

Chromatin immunoprecipitation (ChIP)

Following the ChIP Kit protocol (Millipore), ChIP assays were performed using antibodies against an IgG control (2729, Cell Signaling Technology) and STAT4 (6775, Cell Signaling Technology). In brief, 2×10^6 cells were cross-linked with formaldehyde to covalently link chromatin proteins with nucleic acids. The cross-linked cells were then lysed to isolate the nuclei, and nuclear extracts containing chromatin were obtained. Using STAT4 antibodies, the target chromatin proteins were selectively immunoprecipitated, forming antigen-antibody complexes. After washing away non-specifically bound proteins and nucleic acids, the precipitated complexes were eluted. The cross-linked nucleic acids and proteins were then separated and reverted to their original states. DNA was extracted from the precipitates, and qPCR was used to measure enrichment compared to input relative to either a no-antibody or IgG control.

Luciferase reporter assay

The promoter capabilities of the SHH promoter region, located 2000 bases upstream of the 5'UTR, were assessed using the Dual-Luciferase expression assay (Vazyme, Nanjing) according to the manufacturer's instructions. Briefly, SHH promoter constructs were cloned into the pGL3-promoter vector, and HEK293T cells were transiently transfected with a pGL3 vector, a Renilla control vector (using a 1:10 dilution), and with or without the pcDNA3 empty vector or the pcDNA3-STAT4 expression vector (Gene Technology Co., Ltd.). The SHH promoter construct sequences for each site were as follows: Site 1 (860–873): TTTCTGGAAATTTT, SHH-MUT1: TTGCTAGACATCGT; Site 2 (935–948): CTTCTAAGATGCCC, SHH-MUT2: CTGCTCAGCTGATC; Site 3 (1020–1030): TTTCCCTTGAAAATT, SHH-MUT3: TTGCCGTGCAACCT; Site 4 (1110–1123): TTGCTAGGATAGAT, SHH-MUT4: TTACTIONGCTAACT. Transfections were performed in 24-well plates using 20 μL Trans buffer, 0.16 μg plasmid, and 0.5 μg DNA per well. After 48 h, cells were harvested and Firefly and Renilla

luciferase activities were measured using a microplate luminometer (BioTek Synergy HTX). Data are presented as relative luciferase units (RLUs) indicating Firefly activity/Renilla activity and represent an average of three independent transfections.

Statistical analysis

All data are presented as mean \pm standard error of the mean (SEM), with each experiment repeated three times. Kolmogorov-Smirnov test was employed to assess the normality of the data. For comparisons between the two groups, the Student's t-test is utilized when the continuous variables are normally distributed. Conversely, the Mann-Whitney test is applied when the data do not follow a normal distribution. In cases involving multiple comparisons, data were analyzed using one-way analysis of variance (ANOVA) with a Tukey's multiple comparisons test for normally distributed data and Kruskal-Wallis test for non-normally distributed data. Moreover, we established the binary logistic regression models, and next used the Pearson's test for the correlation analysis. A p-value less than 0.05 was considered statistically significant. Graphs were generated using GraphPad Prism 5 software (GraphPad Software Inc., CA, USA).

Results

Intraventricular injection of rWIF-1 exacerbates cognitive dysfunction and increases mood abnormalities in the TLR7-induced lupus model

Environmental factors play a role in the pathogenesis of SLE, leading to dysfunctions in both the innate and adaptive immune systems. We previously characterized the behavioral phenotype of a mouse model induced by the TLR7 agonist IMQ. Following eight weeks of IMQ cream application, these mice exhibited contextual fear memory in a fear conditioning paradigm and impaired spatial memory in the Morris water maze [47]. Consequently, we employed the IMQ murine model to evaluate the effects of rWIF-1 on functional behaviors at various time points in lupus mice (Fig. 1A). Despite an observed increase in serum anti-dsDNA, IgG, and proteinuria in IMQ-treated mice, we found no significant changes after intraventricular rWIF-1 treatment, suggesting that rWIF-1 does not significantly enhance the B cell inflammatory response or mitigate renal tissue damage (Fig. S1A).

Throughout the experiment, the general condition of the mice was monitored. Mice receiving rWIF-1 injections exhibited lower body weight and higher coat scores after eight weeks (Fig. S1B-C). To evaluate anxiety and depression, the Open Field Test (OFT) and Elevated Plus Maze (EPM) were utilized [48]. Anxious mice tend to avoid exploration and prefer safer locations, such as the outer perimeter of the OFT or the closed arm of the EPM. At week 4, the percentage of time spent in

the center zone and the distance traveled in the center in the OFT, as well as the percentage of time in the open arm and open arm entries in the EPM, were significantly lower in the IMQ+rWIF-1 group compared to the IMQ+PBS group (2.754% vs. 6.494%, $p < 0.05$; 8.909% vs. 14.090%, $p < 0.05$; 5.936% vs. 20.69%, $p < 0.05$; 1.500 vs. 2.700, $p < 0.05$, respectively; Fig. S1D-G). These behavioral changes persisted through weeks 6 and 8, indicating that rWIF-1 injections exacerbated depressive and anxious behaviors in IMQ mice (Fig. 1B-E, S1D-G).

Cognitive function was assessed using the Y-maze and contextual fear conditioning tests [49]. To evaluate spatial memory, the spontaneous alternation rates in the Y-maze were significantly lower in the IMQ+rWIF-1 group than in the IMQ+PBS group from weeks 4 to 8 ($P < 0.05$) (Fig. 1F, G, S1H, I). In the fear conditioning test conducted at week 8, the rWIF-1 group exhibited decreased freezing time during the retention test compared to the IMQ+PBS group ($P < 0.05$), indicating an impairment in hippocampus-dependent fear memory. However, there was no significant difference in the freezing percentage in response to auditory stimuli between the rWIF-1 and PBS-treated IMQ mice (Fig. 1H). Thus, the fear conditioning test suggests that rWIF-1 may affect long-term hippocampus-dependent fear memory but not amygdala-dependent fear memory [50] in lupus mice. In summary, these results indicate that rWIF-1 induces anxiety-like and depression-like behaviors, as well as impairments in spatial and fear memory, in IMQ-induced lupus mice.

Brain-delivered AAV-shWIF-1 ameliorates NPSLE-like behaviors in MRL/lpr lupus-prone mice

MRL/lpr mice develop an "autoimmunity-associated behavioral syndrome" [51] as early as five weeks of age, which is suggested to mimic NPSLE. Compared to the MRL/mpj substrain, a significant number of MRL/lpr mice exhibit deficits in emotional reactivity, motivated behavior, and learning/memory [52–56]. In order to further clarify the role of endogenous WIF-1, we conducted AAV-mediated WIF-1 knockdown in the cerebral lateral ventricles of MRL/lpr mice at 9–10 weeks of age, the starting point of our treatment protocol. WIF-1 expression levels in brain tissues were significantly reduced in the MRL/lpr+shWIF-1 group compared to the MRL/lpr+Vector group ($P < 0.001$) (Fig. S2A).

We then evaluated whether reduced WIF-1 protein expression could protect mood and cognitive functions at 13, 16, and 20 weeks of age (Fig. 2A). The MRL/lpr+Vector group exhibited a significant decrease in body weight compared to the MRL/mpj+Vector group ($P < 0.05$), whereas the MRL/lpr+shWIF-1 group exhibited a moderate increase in body weight, higher than the MRL/lpr+Vector group ($P = 0.0229$) (Fig. S2B). Regarding fur coat scores, WIF-1 knockdown resulted in significant

recovery from the low scores observed in the MRL/lpr+Vector group (Fig. S2C).

The MRL/lpr+shWIF-1 group spent more time and covered a longer distance in central exploration in the OFT test compared to the MRL/lpr+Vector group (At 13 weeks, $P=0.0218$, $P=0.0058$; At 16 weeks, $P=0.0095$, $P=0.0032$; At 20 weeks, $P=0.0448$, $P=0.0495$) (Fig. 2B, C, S2D, E). The EPM test revealed that the MRL/lpr+Vector group had significantly reduced exploration time ($P<0.05$) and frequency in the open arms ($P<0.05$) compared to the MRL/mpj+Vector group from 13 weeks of age. However, the MRL/lpr+shWIF-1 group exhibited less anxiety and depression throughout the experiment (Fig. 2D, E, S2F, G).

We then proceeded to assess cognitive functions using the Y-maze spontaneous alternation task. AAV-shWIF-1-treated mice showed a significant increase in spontaneous alternation ratios compared to MRL/lpr+Vector mice (At 13 weeks, $P=0.0100$; At 16 weeks, $P=0.0095$; At 20 weeks, $P=0.0002$) (Fig. 2F, G, S2H, I). Additionally, the MRL/lpr+shWIF-1 group demonstrated a significant recovery in contextual fear freezing behavior, but no significant difference in the freezing percentage in response to auditory stimuli was found (Fig. 2H), indicating an improvement in hippocampus-dependent long-term memory. Taken together, these findings indicate that knocking down WIF-1 alleviates neurobehavioral abnormalities and cognitive dysfunction in MRL/lpr mice.

Reducing WIF-1 levels improves neuronal degeneration and alleviates BBB damage in lupus mice

Given that the hippocampus and medial prefrontal cortex (mPFC) are crucial regions for emotion and cognition [57–59], and that decreased BBB function has been observed in lupus-prone mice (CReCOM, NZB/W-F1, MRL/lpr) at the disease stage [14, 26, 60], we investigated BBB integrity in these brain regions following WIF-1 intervention. Western blot analysis revealed that AAV-shWIF-1 interference significantly reduced albumin deposition (~1.45-fold) and increased the levels of ZO1 and occludin proteins (~1.69-fold and ~1.44-fold, respectively) in the hippocampus compared to MRL/lpr+Vector mice (Fig. 3A). Conversely, rWIF-1 injection in IMQ mice resulted in opposite effects (Fig. S3A). Disrupted BBB was also evident in the mPFC (Fig. S3B, C).

We further examined the histopathological structure of the hippocampus regions (CA1 and CA3) and the dentate gyrus (DG). Consistent with previous reports [39], the CA1, CA3, and DG areas in the MRL/lpr+Vector group exhibited severe disorganisation, nerve cell degeneration, necrosis, and disintegration. In contrast, the MRL/lpr+shWIF-1 group showed regular and neatly arranged neurons with limited neuronal shrinkage (Fig. 3B). In the IMQ model, rWIF-1 injection exacerbated neuronal

degeneration and death (Fig. S3D). Additionally, Fluoro-Jade B (FJB) labelling, which stains degenerating neurons [61], confirmed decreased neuronal injury in the hippocampus following AAV-shWIF-1 treatment in MRL/lpr mice (Fig. 3C). The IMQ+rWIF-1 group exhibited the highest level of FJB labelling, indicating that reducing rWIF-1 could aggravate neuronal degeneration in lupus mice (Fig. S3E).

The persistence of high levels of pro-inflammatory cytokines is associated with the development of BBB dysfunction [62]. We found that elevated levels of TNF- α and IL-6 in the hippocampal region were significantly reduced in the MRL/lpr+shWIF-1 group (Fig. 3D, E). Notably, we found that the number of CD45^{hi}CD11b⁻ cells in the hippocampus significantly increased in MRL/lpr mice but decreased markedly following shWIF-1 treatment (Fig. 4A, S4B). These findings further confirm that shWIF-1 significantly ameliorates BBB injury and inhibits the infiltration of peripheral lymphocytes. Conversely, the IMQ+rWIF-1 group exhibited higher TNF- α and IL-6 levels than the IMQ+PBS group (Fig. S3F, G), as well as an increased number of CD45^{hi}CD11b⁻ cells (Fig. S4A, B). These *in vivo* results suggest that WIF-1 exacerbates lupus-induced hippocampal BBB impairment, contributing to neuronal degeneration and neuroinflammation.

WIF-1 aggravates microglial overactivation in the hippocampus of murine lupus

Recent studies have indicated that neuroinflammation is a primary pathogenic factor in NPSLE, with microglia being key cells in the inflammatory response [63, 64]. Given WIF-1's effect on increasing levels of inflammatory markers (TNF- α and IL-6) in the lupus-prone hippocampus, we explored the accumulation of activated microglia in the damaged area. Microglia were defined as CD45^{lo}CD11b⁺, and pro-inflammatory microglia as CD45^{lo}CD11b⁺CD86⁺. Compared with MRL/mpj+Vector mice, the number of microglia was elevated in the hippocampal region of MRL/lpr+Vector mice, along with a significant increase in the percentage of CD86⁺ pro-inflammatory microglia (Fig. 4A, B). The percentage of CD86⁺ microglia in the MRL/lpr+shWIF-1 group decreased to levels comparable to the MRL/mpj+Vector group (Fig. 4B). In contrast, exogenous injection with rWIF-1 resulted in a large accumulation of CD86⁺ microglia in the hippocampus of IMQ mice (Fig. S4C).

Excessive synaptic pruning is observed in microglial overactivation in lupus mice brains, in addition to high levels of the microglial activation marker CD86 [39, 65]. We further evaluate WIF-1's effect on synaptic engulfment by microglia *in vivo*. Imaging and quantitative analysis revealed that the number of PSD95⁺ puncta within IBA-1⁺ microglia was significantly lower in

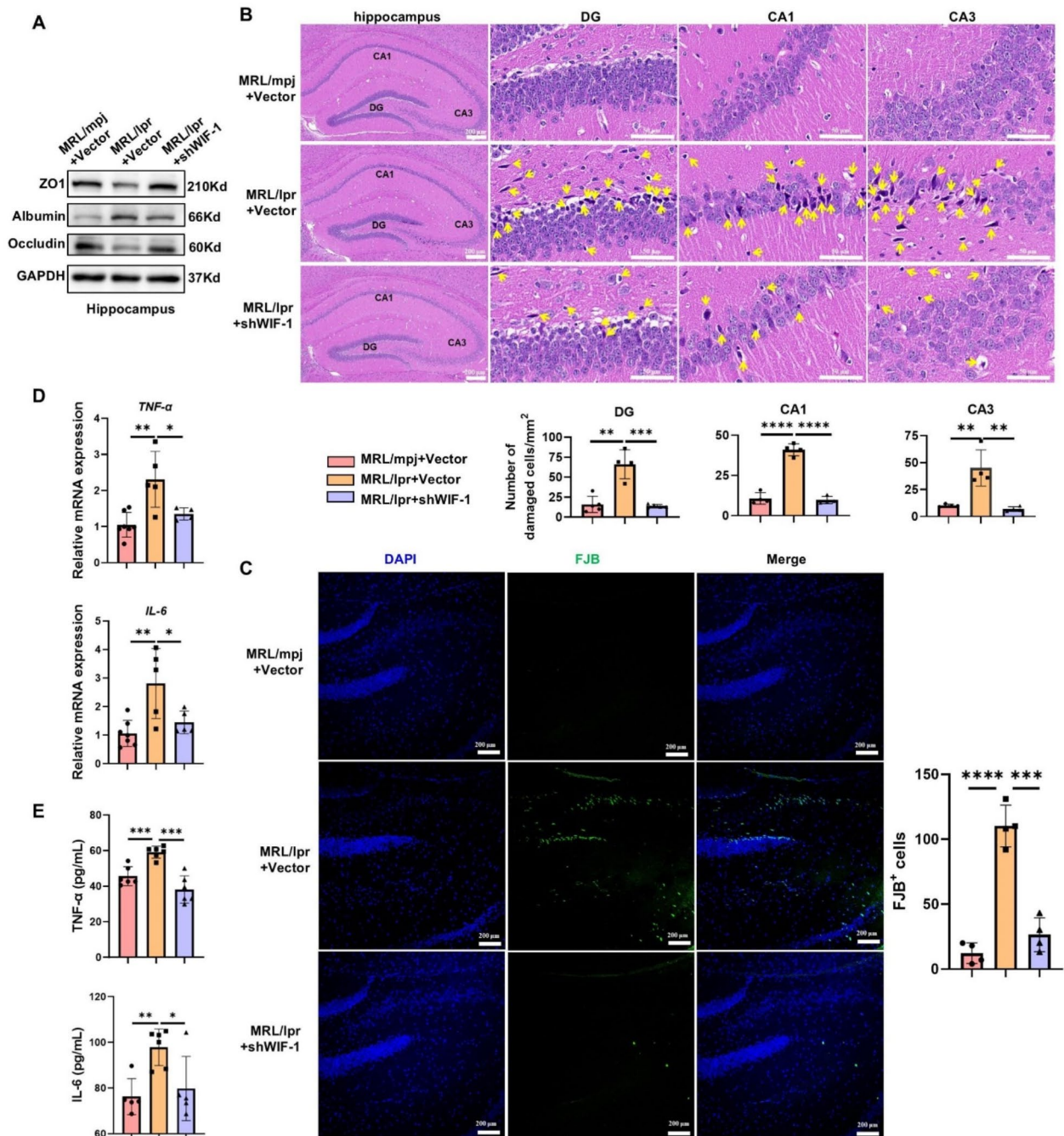


Fig. 3 Reduction of WIF-1 in the brain of MRL/lpr mice alleviates neuronal degeneration and BBB damage. **(A)** Western Blot (WB) analysis assesses the expression of albumin and tight junction proteins ZO1 and Occludin in the hippocampus. **(B)** Hematoxylin-Eosin staining (H&E) reveals the pathological condition of the hippocampal region, $n=4$, bar = 200–50 μm . **(C)** Fluoro-Jade B (FJB) assessment of hippocampal neuronal death, bar = 200 μm . **(D, E)** ELISA and q-PCR detect levels of inflammatory factors TNF- α and IL-6 in the hippocampus. *: $P < 0.05$; **: $P < 0.01$; ***: $P < 0.001$; ****: $P < 0.0001$

MRL/lpr+shWIF-1 mice than in MRL/lpr+Vector mice (Fig. 4C). Western blot analysis also showed decreased expression of microglia markers IBA-1 and phagocytosis marker LAMP1 in the hippocampus of the MRL/lpr+shWIF-1 group, along with a significant increase in hippocampal synaptic markers PSD95 and SYN1

expression (Fig. 4D). Additionally, in the IMQ model, the IMQ+rWIF-1 group showed a significant increase in the percentage of LAMP1⁺ microglia compared to the IMQ+PBS group (Fig. S4D). In the hippocampal regions, rWIF-1 significantly increased LAMP1 and IBA-1 protein expression, while decreasing PSD95 and SYN1

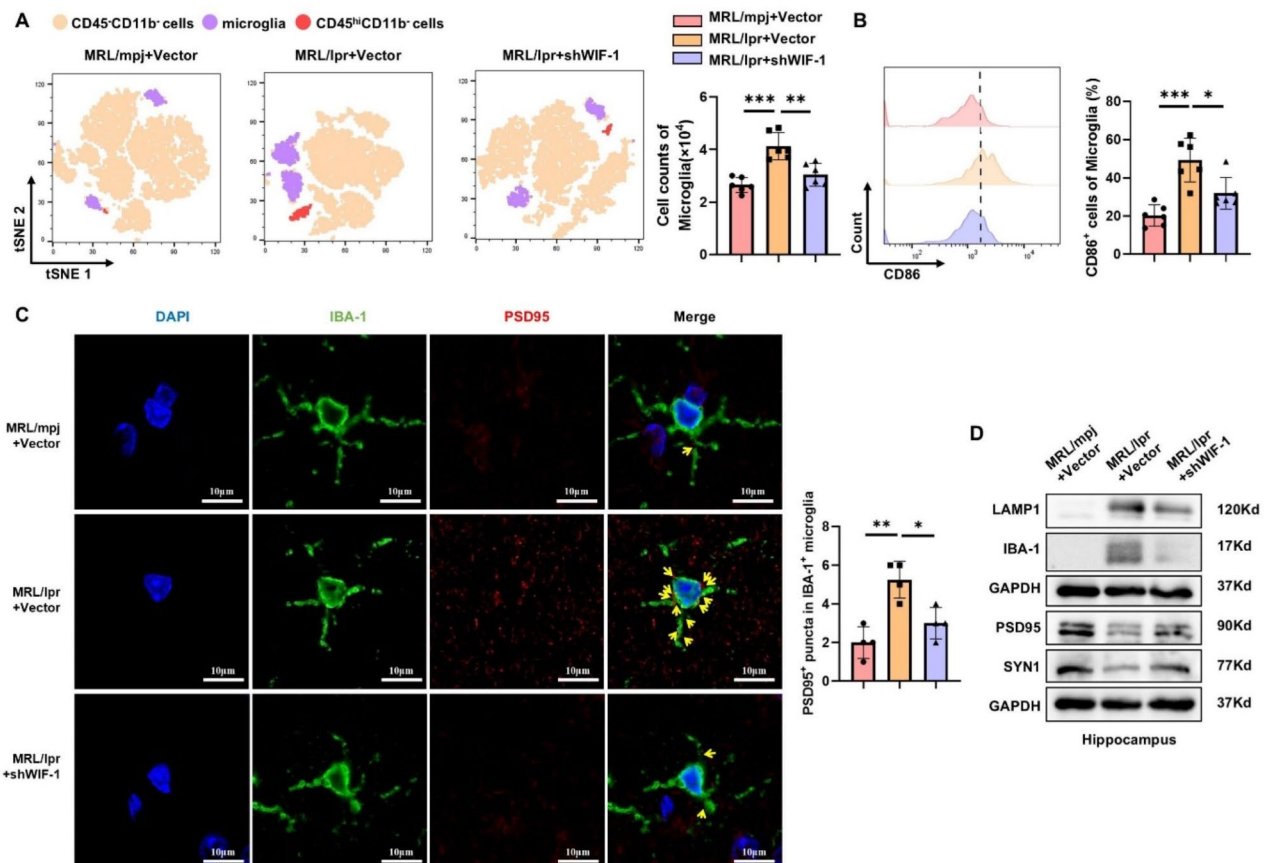


Fig. 4 Knockdown of WIF-1 mitigates the proliferation and activation of microglial cells in MRL/lpr mice. **(A)** tSNE representation highlighting identified hippocampus cell clusters. Flow cytometry quantifies the number of microglial cells, $n=6$. **(B)** Flow cytometry assesses the expression of activation protein CD86 in microglial cells, $n=6$. **(C)** Immunofluorescence co-localization of microglial cells (IBA-1) with PSD95 in the hippocampus, bar = 10 μ m, $n=4$. **(D)** WB assesses the expression of LAMP1, IBA-1, and hippocampal synaptic markers PSD95 and SYN1 in the hippocampus. *: $P < 0.05$; **: $P < 0.01$; ***: $P < 0.001$; ****: $P < 0.0001$

expression (Fig. S4E). Similar changes in protein expression were observed in the mPFC of lupus mice (Fig. S4F). These findings suggest that WIF-1 exacerbates microglial overactivation in lupus mice, leading to abnormal pruning of neuronal synapses.

WIF-1 mediates excessive microglial activation associated with dysregulation of SHH signaling

At the early stages of NPSLE, microglial activation may be a key initiating event [22, 26]. It is known that human WIF-1 protein binds sonic hedgehog (SHH) with high affinity, effectively inhibiting its downstream signaling [66]. The activation of SHH signaling pathway is helpful to maintain BBB integrity [67] and promotes macrophage polarization towards an anti-inflammatory phenotype [68, 69]. In order to ascertain whether microglial SHH plays a crucial role in the exacerbation of NPSLE caused by WIF-1, we first investigated the correlation between SHH molecules and microglia. The results demonstrated a negative correlation between the protein expression

levels of SHH and alterations in the microglial ratio of hippocampal samples in MRL/lpr and IMQ-induced mice (Fig. 5A). Subsequently, immunofluorescence experiments revealed that SHH was distributed around microglia in the hippocampal tissue of NPSLE mice. Additionally, a significant increase in SHH distribution near microglia was observed following the intraventricular injection of shWIF-1 (Fig. 5B). These findings indicate that the regulation of microglial abnormalities by WIF-1 is closely associated with the SHH signaling pathway. Furthermore, we examined the impact of WIF-1 combined with the SHH signal agonist purmorphamine (PUR) on microglial activation and BBB integrity in vitro.

CCK8 assays showed that rWIF-1 concentrations below 5 μ g/mL did not affect the proliferative activity of BV2 murine microglia cells (Fig. S5A). We selected a concentration of 1 μ g/mL for further experiments. After treating BV2 cells with rWIF-1 for 24 h, a significant increase in the proportion of pro-inflammatory marker CD86 was observed (Fig. 5C). LAMP1, a

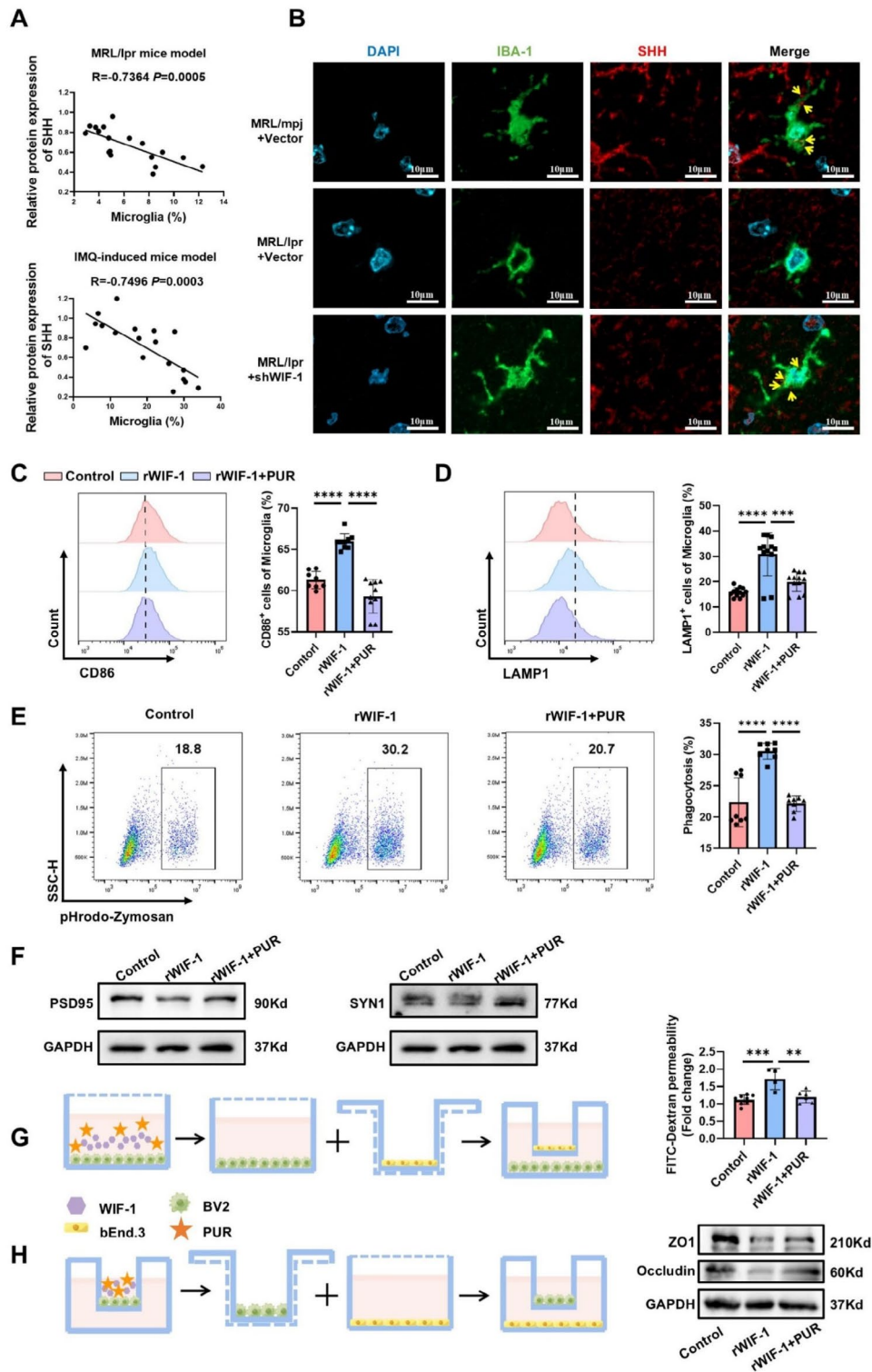


Fig. 5 PUR alleviates abnormal activation of BV2 cells and BBB damage. **(A)** Correlation between the protein expression level of SHH with microglial ratio of hippocampal samples in two types from lupus mice. **(B)** Immunofluorescence was used to detect the co-location of SHH and microglia, bar = 10 μ m, $n = 4$. **(C, D)** Flow cytometry detects the expression of CD86 and LAMP1 in BV2 cells. **(E)** Flow cytometry evaluates the ability of BV2 cells to engulf yeast glucans. **(F)** BV2 and HT22 cells were co-cultured at a 1:3 ratio. WB examines the levels of PSD95 and SYN1 expressed by HT22 cells after co-culture. **(G)** Fluorescence intensity of FITC-Dextran was detected in an in vitro BBB permeability assay. **(H)** WB assesses the expression levels of ZO1 and Occludin in bEnd.3 cells in an in vitro BBB model. *: $P < 0.05$; **: $P < 0.01$; ***: $P < 0.001$; ****: $P < 0.0001$

phagocytosis-specific marker, also showed increased expression in rWIF-1-treated cells (Fig. 5D). The percentage of microglia with internalized fluorescent bioparticles significantly increased after exposure to pHrodo™ green zymosan bioparticles in the presence of rWIF-1 (Fig. 5E).

We subjected rWIF-1-stimulated BV2 and HT22 cells to cell-cell interaction models to further evaluate the effect of rWIF-1 on microglia-mediated synaptic pruning. The rWIF-1 group showed decreased levels of PSD95 and SYN1 in HT22 cells compared to the control group (Fig. 5F). Brain endothelial cells (ECs) tightly line the blood vessels in the CNS, forming a protective structural barrier [70]. We investigated whether rWIF-1 treatment affected murine brain ECs (bEnd.3 cells) injury in a bEnd.3 cells/BV2 cells co-culture. In a BBB permeability assay, pretreatment of BV2 cells with rWIF-1 significantly increased the fluorescence intensity of FITC-Dextran in the lower chamber (Fig. 5G). Western blot analysis revealed that rWIF-1 pre-treatment decreased the expression of occludin and ZO1 in co-cultured bEnd.3 cells. However, pre-treatment with PUR (1.5 μmol/L) significantly blocked rWIF-1-induced excessive activation of microglia (Fig. 5H). These results indicate that rWIF-1 induces abnormal activation of microglia by inhibiting SHH signaling, leading to disruption of the BBB barrier.

WIF-1 inhibits SHH expression through CRYAB /STAT4 pathway in overactivated microglial cells

To investigate the potential mechanism by which WIF-1 regulates SHH, we conducted RNA-seq analysis on BV2 cells from both the Control group and the rWIF-1 group. We further screened the downstream targets regulated by WIF-1, combining our findings with a literature review (Fig. 6A). Differential expression analysis revealed 71 differentially expressed genes (DEGs) (Supplementary Table 1), among which 10 genes, including CRYAB, exhibited the most significant differences (Fig. 6B, C).

Previous studies have implicated CRYAB in apoptosis and the regulation of neuronal survival in the nervous system [71]. We performed Western blot assays to validate the protein expression levels of CRYAB in rWIF-1-induced BV2 cells and hippocampal tissues from MRL/lpr mice and IMQ-treated mice (Fig. 6D). Subsequently, we used siRNA to knock down the elevated expression of CRYAB induced by rWIF-1 in BV2 cells (Fig. 6E). This knockdown resulted in a reduction of CD86⁺ pro-inflammatory microglia and decreased phagocytic activity (Fig. 6F-H). Concurrently, the expression of SHH protein also increased (Fig. 6E). These results suggest that rWIF-1 activates microglia by upregulating CRYAB and downregulating SHH.

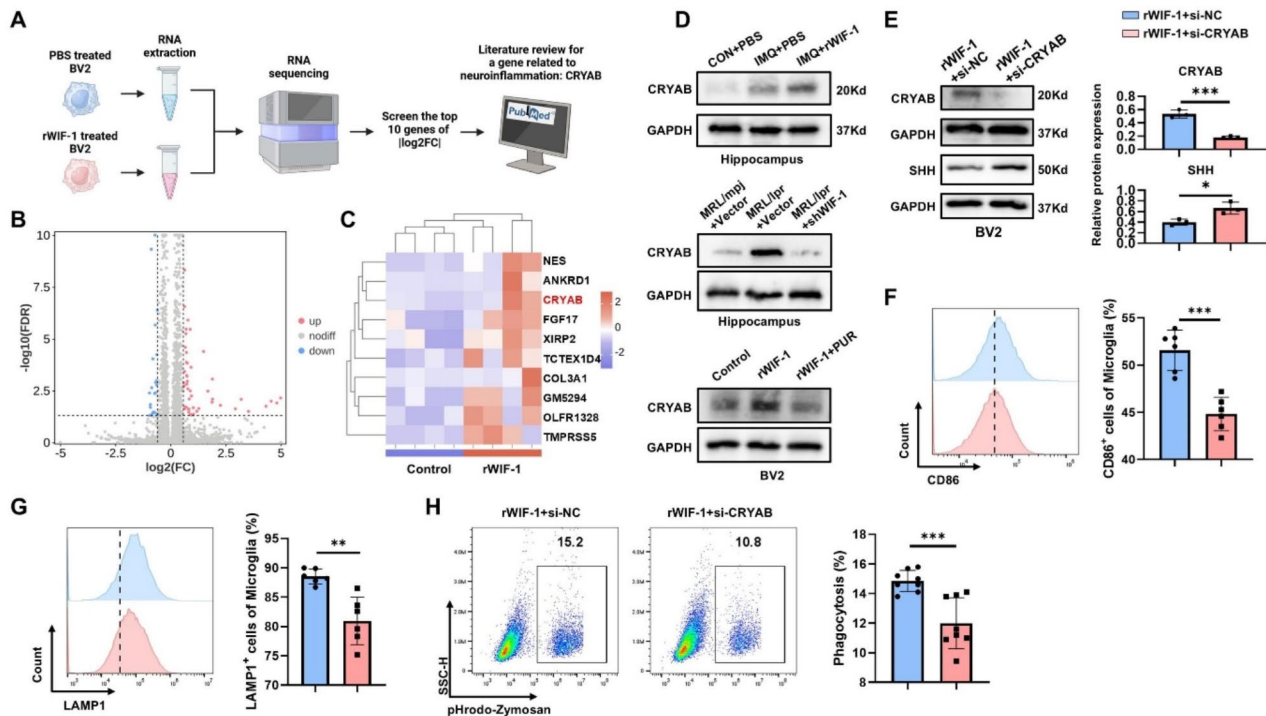


Fig. 6 CRYAB mediates abnormal activation of BV2 cells. **(A)** WIF-1 downstream target gene screening strategy map created with BioRender.com. **(B)** Volcano plot from RNA-seq analysis depicts differentially expressed genes in microglia following rWIF-1 stimulation. **(C)** Heat map shows the top 10 genes in $|\log_2(\text{FC})|$. **(D)** WB validates CRYAB expression in the hippocampus of both lupus mouse models and BV2 cells. **(E)** WB confirms the knockdown effect of si-CRYAB transfection in BV2 cells and assesses the expression of SHH. **(F, G)** Flow cytometry assesses the expression of CD86 and LAMP1 in BV2 cells. **(H)** Flow cytometry evaluates the engulfing ability of BV2 cells. *: $P < 0.05$; **: $P < 0.01$; ***: $P < 0.001$

It is known that SHH expression is regulated by transcription factors [72, 73]. To explore the upstream molecules affecting SHH expression, we used the JASPAR database to predict transcription factors (TFs) regulating the SHH promoter and evaluated the expression levels of the top 8 potential TFs via qRT-PCR (Fig. 7A). STAT4 and EGR2 were selected for further investigation. Luciferase reporter gene assays revealed that only STAT4 suppressed the activity of the SHH promoter (Fig. 7B), and ChIP assays confirmed the direct binding of STAT4 to SHH (Fig. 7C).

Furthermore, JASPAR predicted possible binding sites of STAT4 in the SHH promoter region (Fig. 7D). To

explore this mechanism, we constructed plasmids containing the wild-type (WT) SHH promoter region and mutant plasmids targeting four binding sites (MUT1, MUT2, MUT3, MUT4). Dual-luciferase assays demonstrated that STAT4 overexpression significantly inhibited luciferase activity when co-transfected with SHH-WT, SHH-MUT1, SHH-MUT2, and SHH-MUT4. However, co-transfection with SHH-MUT Total, containing mutations in all four sites, showed no significant change in luciferase activity. Co-transfection with SHH-MUT3 and STAT4 overexpression did not alter luciferase activity

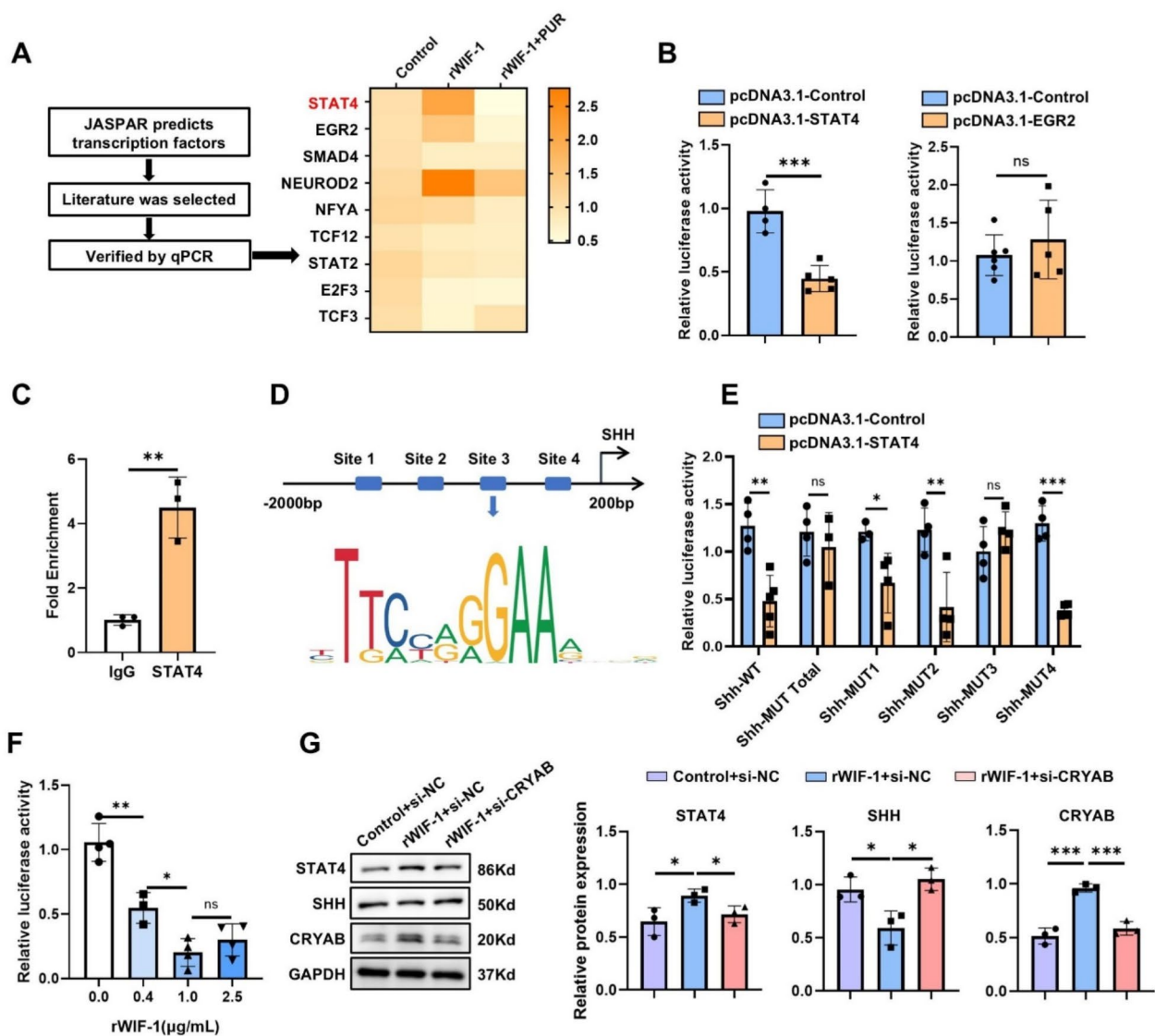


Fig. 7 CRYAB/STAT4 is a key mediator of WIF-1 in regulating the SHH signaling pathway. **(A)** Potential transcription factors regulating SHH were predicted by JASPAR, with qPCR validating their expression patterns. **(B)** The Luciferase reporter gene validates transcription factors. **(C)** ChIP assay indicates the binding of STAT4 to the SHH promoter in BV2 cells. **(D, E)** The Luciferase reporter gene demonstrates STAT4 binding to the SHH promoter region at 1020–1030 bp. **(F)** Luciferase reporter gene shows SHH transcriptional activity decreases with increasing WIF-1 concentration. **(G)** WB detects changes in the CRYAB/STAT4-SHH axis. *: $P < 0.05$; **: $P < 0.01$; ***: $P < 0.001$

either, indicating the crucial role of STAT4 in regulating SHH in a specific promoter region (879–892 bp) (Fig. 7E).

Additionally, we treated BV2 cells with different concentrations of rWIF-1 (0.4, 1.0, 2.5 $\mu\text{g}/\text{mL}$) and transfected them with SHH-WT plasmids. As the concentration of rWIF-1 increased, luciferase activity gradually decreased (Fig. 7F), providing further evidence that WIF-1 inhibits SHH signaling through STAT4 regulation. Western blot validation in BV2 cells showed that rWIF-1 treatment significantly increased the expression of CRYAB and STAT4 while reducing SHH expression. However, knocking down CRYAB expression with si-CRYAB eliminated the induction of STAT4 and SHH (Fig. 7G), further confirming that rWIF-1 transcriptionally inhibits SHH expression through the CRYAB/STAT4 pathway.

We also validated the CRYAB/STAT4-SHH axis in the hippocampal and mPFC regions of the IMQ mouse model, as well as in the MRL/lpr mouse model (Fig. S5B, C). These results confirm that the rWIF-1-induced CRYAB/STAT4-SHH axis facilitates microglial overactivation in lupus mice.

Symmetric dimethylarginine alleviates WIF-1-induced microglial aberrant activation and BBB damage, restoring SHH production

Symmetric dimethylarginine (SDMA), a byproduct of protein methylation, has been reported to inhibit STAT4 expression [74]. Thus, we investigated the potential therapeutic effects of SDMA on NPSLE in vitro. CCK8 assays showed that SDMA at concentrations below 2.5 μM does not affect the proliferative activity of BV2 cells (Fig. 8A). We selected 2.5 μM SDMA for subsequent experiments.

Validation of the CRYAB/STAT4-SHH pathway in BV2 cells revealed that SDMA reduces the expression of STAT4 while increasing SHH expression, without significantly affecting CRYAB (Fig. 8B). Furthermore, pretreatment with SDMA eliminated rWIF-1-induced inflammatory polarisation and phagocytic activity (Fig. 8C–E). The rWIF-1+SDMA group showed a reduction in the abnormal pruning effect of BV2 on neurons compared to the rWIF-1 group, including increased expression of PSD95 and SYN1 (Fig. 8F). Additionally, tight junction proteins ZO1 and occludin significantly increased in the rWIF-1+SDMA group, leading to decreased BBB permeability (Fig. 8G, H). In conclusion, SDMA alleviates BV2 abnormal activation and BBB damage by inhibiting STAT4 expression.

Discussion

NPSLE is the second leading cause of death in SLE patients [2]. Early diagnosis is challenging, clinical treatments are limited, and its pathogenesis remains unclear. Among its diverse clinical phenotypes, cognitive

dysfunction is the most common [75], significantly affecting patients' physical and mental health and their quality of life. The identification and mechanistic study of biomarkers are crucial for the diagnosis and treatment of NPSLE. Based on intraventricular treatment in murine NPSLE models, we further elucidated the role and molecular mechanism of the potential biomarker WIF-1 in the cognitive impairment observed in lupus mice.

Initially, we confirmed the effect of WIF-1 on cognitive dysfunction in MRL/lpr and IMQ-induced lupus mouse models. We injected recombinant WIF-1 (rWIF-1) or AAV-SHIF-1 into the lateral ventricle to increase or reduce WIF-1 expression in the brains of lupus mice, confirming that WIF-1 may be a key factor inducing cognitive dysfunction, BBB damage, and microglial activation in lupus mice. In addition, we evaluated the effect of intraventricular injection of shWIF-1 on the peripheral immune environment. A semi-quantitative planar antibody microarray analysis for murine serum revealed a significant decrease in T cell-related cytokines IL-4, IL-10 and macrophage cytokine MIP-1 α in the MRL/lpr+shWIF-1 group (Fig. S6A). We further confirmed such marked gene expression in Th2 cells and macrophages, while no significant effects were observed on Th1, Th17, Treg cell subsets or B cells (Fig. S6B–E). These results suggest that intracerebroventricular injection of shWIF-1 may reduce peripheral inflammation by reducing Th2 cells and macrophages. This further validated the reduction of infiltrating CD45^{hi}CD11b⁻ cells in the hippocampus and the alleviation of BBB damage. Current studies indicate that intraventricular injection of PGE2 can influence the proliferation of blood lymphocytes in response to T cell mitogens, suggesting the potential involvement of the central nervous system in the functional regulation of the peripheral immune system [76]. Further research and exploration are required to validate these findings.

Notably, in the early stages of lupus onset (4 weeks post-IMQ treatment and 13 weeks in MRL/lpr mice), there was a marked exacerbation of anxiety, depression-like behaviors, and cognitive impairment, which persisted. Behavioral deficits in the MRL/lpr substrain have been observed as early as 7 weeks of age [77], coinciding with the emergence of humoral autoimmunity but preceding generalized lymphadenopathy, arthritis, glomerulonephritis, and skin lesions. These findings suggest that cognitive impairment may precede typical lupus symptoms. It is significant that both increasing and decreasing WIF-1 levels can substantially regulate BBB damage and cognitive dysfunction in the early stages of lupus, with consistent results observed in both induced and autoimmune lupus mouse models. This indicates that WIF-1 plays a crucial role in the early induction stage of NPSLE, supporting its feasibility as an early diagnostic

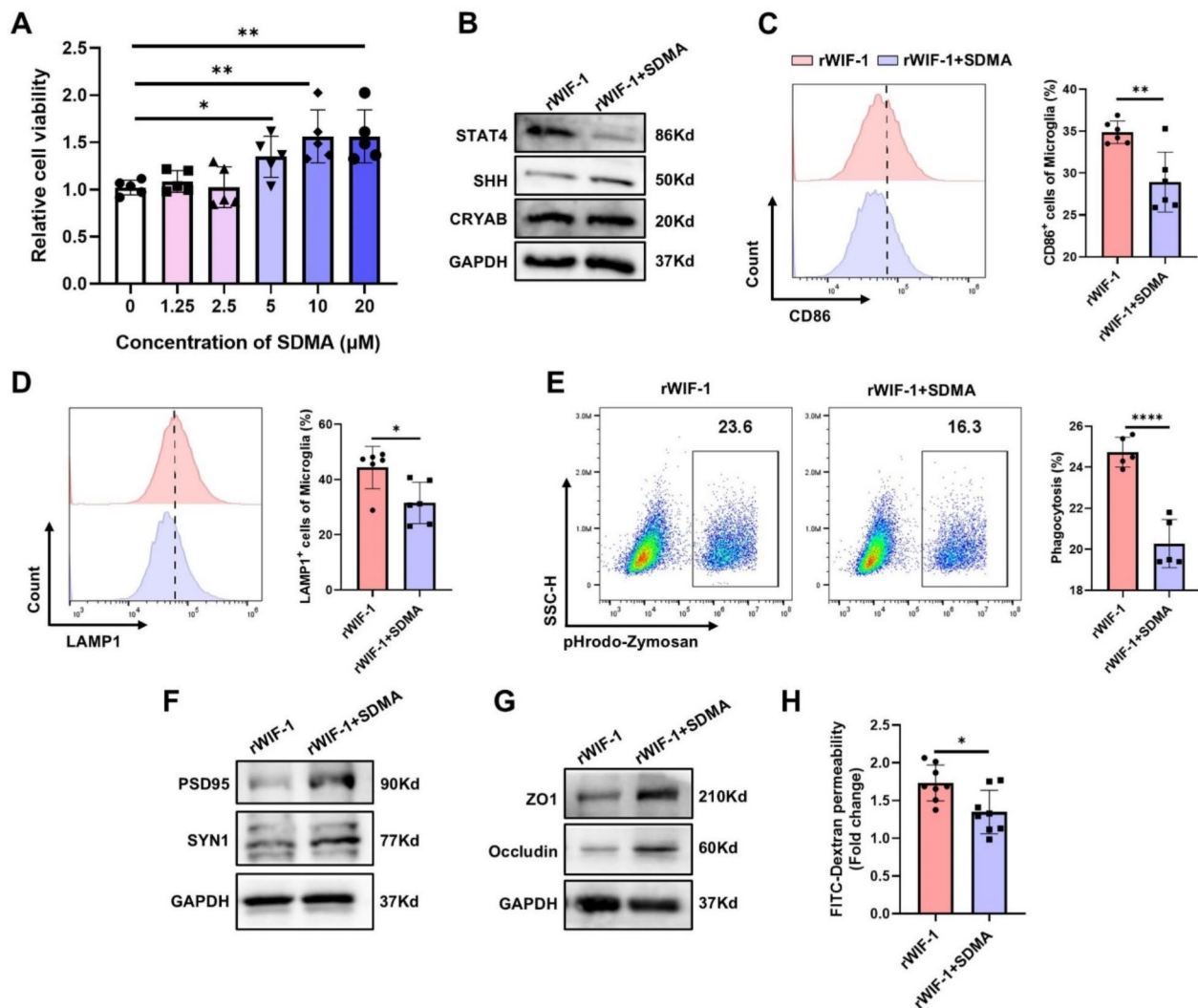


Fig. 8 SDMA alleviates BV2 activation and BBB damage by inhibiting STAT4. **(A)** CCK8 assay evaluates SDMA impact on BV2 cell proliferation. **(B)** WB detects the expression changes in the CRYAB/STAT4-SHH axis after SDMA treatment in BV2 cells. **(C, D)** Flow cytometry detects the expression of CD86 and LAMP1 in BV2 cells. **(E)** Flow cytometry assesses the ability of BV2 cells to engulf yeast glucan. **(F)** WB detects PSD95 and SYN1 expression levels in the co-culture model of cells. **(G)** WB detects the expression of ZO1 and Occludin in an in vitro BBB model. **(H)** In vitro BBB permeability assay. *: $P < 0.05$; **: $P < 0.01$; ***: $P < 0.001$; ****: $P < 0.0001$

marker. WIF-1 has been associated with nerve injury and behavioural disorders in human schizophrenia [78] and Alzheimer's disease (AD) [79], further suggesting that WIF-1 may be a critical factor in the brain damage associated with NPSLE.

The loss of BBB integrity is a widely accepted mechanism of SLE-related brain injury [80]. Studies have shown that activated microglia, macrophages in brain tissue, disrupt BBB permeability during sustained inflammation [22], indicating that microglial activation may be a key initial event in NPSLE. Our results confirm that WIF-1 induces the pro-inflammatory phenotype of microglia and enhances their phagocytic activity through the CRYAB/STAT4-SHH signaling pathway, thus disrupting

BBB integrity and leading to neuronal death. This plays a significant role in the pathogenesis of lupus encephalopathy. We elucidated the novel molecular mechanism of WIF-1, instead of participating in brain injury by inhibiting β -catenin signaling pathway [39]. As a small heat shock protein, CRYAB's abnormal expression may be related to diseases such as AD and Parkinson's disease (PD) [81, 82], and it is known to play a role in regulating brain injury and inflammatory responses [83, 84]. CRYAB is reported to be regulated by PI3K/Akt signal transduction [85] and p38 MAPK dependence [81] in AD, with the interaction between CRYAB and STAT3 in astrocytes involved in regulating neuroinflammation [71]. We found for the first time that CRYAB can positively regulate

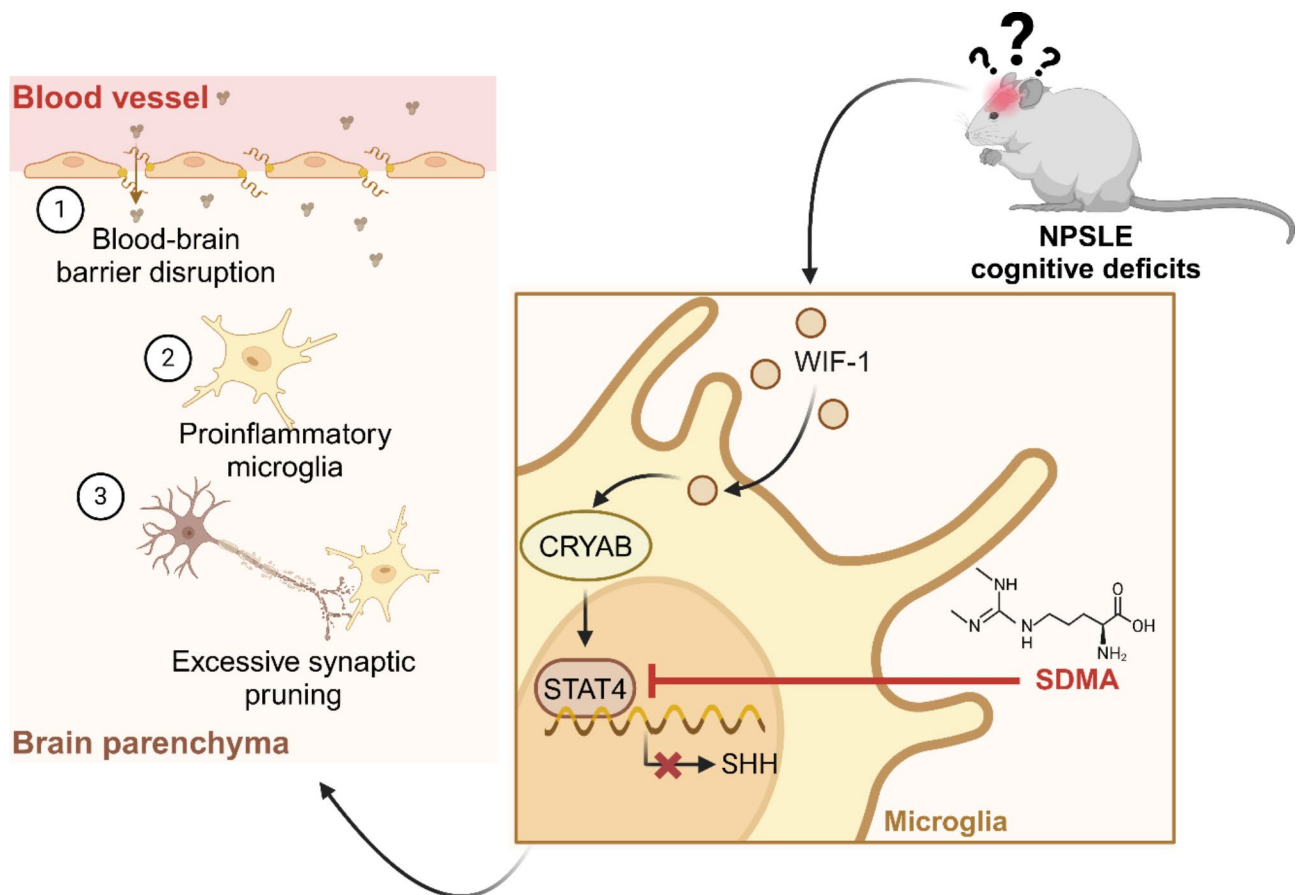


Fig. 9 Mechanism diagram of abnormal neurobehavioral state and cognitive impairment induced by WIF-1 in lupus mice created with BioRender.com

the expression of STAT4 in microglia, and the specific molecular mechanism requires further exploration.

STAT4, a pro-inflammatory gene, is mainly expressed in microglia in multiple sclerosis [86] and autoimmune encephalomyelitis [87]. As a negatively regulated transcription factor, STAT4 blocks the MAPK pathway by inhibiting KISS1, playing an important role in regulating oxidative damage, inflammation, and neuronal apoptosis induced by PD [88]. Currently, there is a lack of exploration into the regulatory function of STAT4 in NPSLE. Our further study confirmed that STAT4 inhibited the transcription of SHH in microglia. SHH signal transduction is closely related to CNS morphogenesis, and abnormal regulation of the SHH signaling pathway may lead to various neurological disorders [89]. SHH signal transduction is involved in maintaining BBB function [90], reducing microglia proliferation [69], and mitigating the inflammatory response [68]. We associated SHH with NPSLE for the first time, observing phenomena consistent with previous reports. The loss of SHH protein is accompanied by aggravated emotional abnormalities, cognitive dysfunction, BBB homeostasis disruption, and abnormal microglial activation.

Recent studies have shown that human WIF-1 protein binds SHH with high affinity and effectively inhibits its signaling activity [66]. Our study demonstrated that the inhibitory effect of WIF-1 on the SHH pathway is related to the regulatory mechanism of STAT4 transcriptional inhibition mediated by CRYAB, which improves our understanding of how WIF-1 suppresses the SHH pathway. Additionally, a review of the literature indicates that Wnt ligands (such as Wnt1, Wnt3a, Wnt4, Wnt5a, Wnt8a, and Wnt9a), Frizzled receptors (Fzd1 and Fzd2), and the low-density lipoprotein receptor-related protein complex (Lrp5/6) are potential interaction partners of WIF-1 [91]. This suggests that WIF-1 may mediate the regulation of the CRYAB/SHH signaling pathway by binding to ligands in NPSLE. This will be further investigated in future research.

In our exploration of therapeutic strategies for NPSLE, we found that SDMA can effectively inhibit STAT4 expression through a literature review [74]. SDMA, a metabolite increased by protein methylation and oxidative stress [92], has levels closely related to glomerular filtration rate [93]. SDMA has been shown to play a potential pathogenic role in cardiovascular and cerebrovascular diseases, with serum SDMA concentrations

significantly increased in dementia patients, reflecting the severity of cognitive impairment [94]. However, it is important to note that serum levels may not reflect the brain's microenvironment. Studies on animal models of learning and memory deficiency found that chronic administration resulted in uniformly decreased SDMA levels in hippocampal and mPFC tissues [95], suggesting that brain SDMA recovery may positively affect the disease. The role of SDMA in brain tissue and its molecular mechanism remain unclear. In vitro, we confirmed that SDMA restores the overactivation of BV2 cells and mitigates BBB damage. These results suggest tissue-specific mechanisms of SDMA's action. Whether brain administration of SDMA has therapeutic effects on lupus encephalopathy requires further exploration.

Conclusions

In summary, this study confirmed that WIF-1 promotes abnormal activation of microglia and induces the destruction of the BBB, thereby exacerbating the development of neurobehavioral abnormalities and cognitive dysfunction in a lupus mouse model. Mechanistically, WIF-1 enhances the expression of CRYAB, subsequently inhibiting SHH by upregulating STAT4 transcription, leading to abnormal activation and increased phagocytosis of microglia (Fig. 9). As an inhibitor of STAT4, SDMA demonstrates significant potential in the treatment of lupus encephalopathy. These findings are instrumental in elucidating the complex pathophysiology of lupus encephalitis, improving our understanding of the relationship between autoimmune diseases and neurological function, and providing a new perspective for future treatment and research.

WIF-1 regulates the overactivation and phagocytosis of microglia through the CRYAB/STAT4-SHH axis and induces BBB damage. SDMA can reverse the abnormal behavior of microglia by inhibiting STAT4.

Abbreviations

NPSLE	Neuropsychiatric systemic lupus erythematosus
BBB	Blood-brain barrier
WIF-1	Wnt-inhibitory factor-1
rWIF-1	Recombinant WIF-1
IMQ	Imiquimod
AAV	Adeno-associated virus
SDMA	Symmetric dimethylarginine
mRNAs	Messenger RNAs
CSF	Cerebrospinal fluid
CNS	Central nervous system
RLUs	Relative luciferase units
OFT	Open Field Test
EPM	Elevated Plus Maze
FJB	Fluoro-Jade B
SHH	Sonic hedgehog
PUR	Purmorphamine
ECs	Endothelial cells
DEGs	Differentially expressed genes
Tfs	Transcription factors
WT	Wild-type

mPFC	Medial prefrontal cortex
AD	Alzheimer's disease
PD	Parkinson's disease

Supplementary Information

The online version contains supplementary material available at <https://doi.org/10.1186/s13075-024-03420-8>.

Supplementary Material 1

Supplementary Material 2

Supplementary Material 3

Acknowledgements

We would like to thank Prof. Tianjiao Xia (Medical school, Nanjing University) and Prof. Lizhi Xu (Medical school, Nanjing University) for helpful guidance on behavioral testing.

Author contributions

LPT, YF, YYH and HD performed conceptualization. LPT, YF and XYX performed methodology, data curation and validation. YF and TSZ performed software formal analysis. TSZ, XYC and CHZ performed investigation. YF performed writing—original draft preparation. LPT and HD performed writing—review and editing and visualization. HD and YYH performed resources, supervision and project administration. JL and HD performed funding acquisition. All authors read and approved the final manuscript.

Funding

This work was supported by the National Natural Science Foundation of China (32070883), and funding for Clinical Trials from the Affiliated Drum Tower Hospital, Medical School of Nanjing University (2022-LCYJ-MS-38), and the Puai Medical Research Fund of Beijing Bethune Charitable Foundation (PAYJ-008), and the Innovative Training Program for Undergraduates of Nanjing University (202410284160Z).

Data availability

All data generated or analysed during this study are included in this published article and its supplementary information files.

Declarations

Ethics approval and consent to participate

All animal experimental procedures were performed under Brazilian Federal Law 1.794/2008 for the scientific use of animals and approved by the Institutional Animal Care and Use Committee of the Affiliated Drum Tower Hospital of Nanjing University Medical School (2023AE01037).

Consent for publication

Not applicable.

Competing interests

The authors declare no competing interests.

Received: 16 July 2024 / Accepted: 16 October 2024

Published online: 23 October 2024

References

1. Kello N, Anderson E, Diamond B. Cognitive dysfunction in systemic lupus erythematosus: a case for initiating trials. *Arthritis Rheumatol*. 2019;71:1413–25.
2. Bendorius M, Po C, Muller S. H. Jeltsch-David. From systemic inflammation to Neuroinflammation: the case of Neurolupus. *Int J Mol Sci*. 2018;19.
3. The American College. Of Rheumatology nomenclature and case definitions for neuropsychiatric lupus syndromes. *Arthritis Rheum*. 1999;42:599–608.
4. Ainiala H, Hietaharju A, Loukkola J, Peltola J, Korpela M, Metsanoja R, Auvinen A. Validity of the new American College of Rheumatology criteria for neuropsychiatric lupus syndromes: a population-based evaluation. *Arthritis Rheum*. 2001;45:419–23.

5. Schwartz N, Stock AD, Putterman C. Neuropsychiatric lupus: new mechanistic insights and future treatment directions. *Nat Rev Rheumatol*. 2019;15:137–52.
6. Khan MI, Qureshi H, Akhtar S, Bae SJ, Hassan F. Prevalence of neuropsychiatric disorders in patients with systemic lupus erythematosus in Pakistan: a systematic review and meta-analysis. *Front Psychiatry*. 2023;14.
7. Monahan RC, Middelkoop HAM, van de Voorde LJJB, Fronczek R, Groenwold RHH, Kloppenburg M, Huizinga TWJ. Steup-Beekman. High prevalence but low impact of cognitive dysfunction on quality of life in patients with lupus and neuropsychiatric symptoms. *Arthritis Care Res*. 2023;75:1017–25.
8. Aranow C, Diamond B, Mackay M. Glutamate receptor Biology and its clinical significance in neuropsychiatric systemic Lupus Erythematosus. *Rheum Dis Clin N Am*. 2010;36:187–.
9. Deijns SJ, Broen JCA, Kruyt ND, Schubart CD, Andreoli L, Tincani A, Limper M. The immunologic etiology of psychiatric manifestations in systemic lupus erythematosus: a narrative review on the role of the blood brain barrier, antibodies, cytokines and chemokines. *Autoimmun Rev*. 2020;19:102592.
10. Lu Y, Chen X, Liu X, Shi Y, Wei Z, Feng L, Jiang Q, Ye W, Sasaki T, Fukunaga K, Ji Y, Han F, Lu YM. Endothelial TFEB signaling-mediated autophagic disturbance initiates microglial activation and cognitive dysfunction. *Autophagy*. 2023;19:1803–20.
11. Zhan R, Meng X, Tian DP, Xu J, Cui HT, Yang JL, Xu YK, Shi MM, Xue J, Yu WW, Hu GF, Li K, Ge XX, Zhang Q, Zhao MM, Du JY, Guo X, Xu WL, Gao Y, Yao CY, Chen F, Chen Y, Shan WX, Zhu YJ, Ji L, Pan B, Yu Y, Li WG, Zhao XY, He QH, Liu XH, Huang Y, Liao SY, Zhou B, Chui DH, Chen YE, Sun Z, Dong ED, Wang YJ, Zheng LM. NAD plus rescues aging-induced blood-brain barrier damage via the CX43-PARP1 axis. *Neuron*. 2023;111.
12. Yue JH, Tan Y, Huan RZ, Guo J, Yang S, Deng M, Xiong YB, Han GQ, Liu L, Liu J, Cheng Y, Zha Y, Zhang JQ. Mast cell activation mediates blood-brain barrier impairment and cognitive dysfunction in septic mice in a histamine-dependent pathway. *Front Immunol*. 2023;14.
13. Kamintsky L, Beyea SD, Fisk JD, Hashmi JA, Omisade A, Calkin C, Bardouille T, Bowen C, Quraan M, Mitnitski A, Matheson K, Friedman A, Hanly JG. Blood-brain barrier leakage in systemic lupus erythematosus is associated with gray matter loss and cognitive impairment. *Ann Rheum Dis*. 2020;79:1580–7.
14. Fan Y, Liu X, Wu J, Ni J, Liang J, Hou Y. Dou. Small molecule compound K-7174 attenuates neuropsychiatric manifestations in lupus-prone mice. *Brain Res*. 2023;1801:148203.
15. Thurgur H, Pinteaux E. Microglia in the neurovascular unit: blood-brain barrier-microglia interactions after Central Nervous System disorders. *Neuroscience*. 2019;405:55–67.
16. Reiss Y, Bauer S, David B, Devraj K, Fidan E, Hattingen E, Liebner S, Melzer N, Meuth SG, Rosenow F, Rueber T, Willems LM, Plate KH. The neurovasculature as a target in temporal lobe epilepsy. *Brain Pathol*. 2023;33.
17. Kang R, Gamdzky M, Lenahan C, Tang J, Tan S, Zhang JH. The dual role of Microglia in Blood-Brain Barrier Dysfunction after Stroke. *Curr Neuroparmacol*. 2020;18:1237–49.
18. Yu Z, Fang X, Liu W, Sun R, Zhou J, Pu Y, Zhao M, Sun D, Xiang Z, Liu P, Ding Y, Cao L. He. Microglia regulate blood-brain Barrier Integrity via MiR-126a-5p/MMP9 Axis during Inflammatory Demyelination. *Adv Sci (Weinh)*. 2022;9:e2105442.
19. Ni K, Zhu J, Xu X, Liu Y, Yang S, Huang Y, Xu R, Jiang L, Zhang J, Zhang W. Ma. Hippocampal activated microglia may contribute to blood-brain barrier impairment and cognitive dysfunction in post-traumatic stress disorder-like rats. *J Mol Neurosci*. 2022;72:975–82.
20. Tang JJ, Jin YC, Jia F, Lv T, Manaenko A, Zhang LF, Zhang ZY, Qi X, Xue YJ, Zhao B, Zhang XH, Zhang JH, Lu JF, Hu Q. Gas6 promotes Microglia Efferocytosis and suppresses inflammation through activating Axl/Rac1 signaling in Subarachnoid Hemorrhage mice. *Translational Stroke Res*. 2023;14:955–69.
21. Stankovic ND, Teodorczyk M, Ploen R, Zipp F, Schmidt MHH. Microglia-blood vessel interactions: a double-edged sword in brain pathologies. *Acta Neuropathol*. 2016;131:347–63.
22. Haruwaka K, Ikegami A, Tachibana Y, Ohno N, Konishi H, Hashimoto A, Matsumoto M, Kato D, Ono R, Kiyama H, Moorhouse AJ, Nabekura J. Wake. Dual microglia effects on blood brain barrier permeability induced by systemic inflammation. *Nat Commun*. 2019;10:5816.
23. Kong X, Zhang Z, Fu T, Ji J, Yang J, Gu Z. TNF-alpha regulates microglial activation via the NF-kappaB signaling pathway in systemic lupus erythematosus with depression. *Int J Biol Macromol*. 2019;125:892–900.
24. Wen J, Chen CH, Stock A, Doerner J, Gulinello M, Putterman C. Intracerebroventricular administration of TNF-like weak inducer of apoptosis induces depression-like behavior and cognitive dysfunction in non-autoimmune mice. *Brain Behav Immun*. 2016;54:27–37.
25. Nomura A, Noto D, Murayama G, Chiba A, Miyake S. Unique primed status of microglia under the systemic autoimmune condition of lupus-prone mice. *Arthritis Res Ther*. 2019;21:303.
26. Nikolopoulos D, Manolakou T, Polissidis A, Filia A, Bertsiaris G, Koutmani Y, Boumpas DT. Microglia activation in the presence of intact blood-brain barrier and disruption of hippocampal neurogenesis via IL-6 and IL-18 mediate early diffuse neuropsychiatric lupus. *Ann Rheum Dis*. 2023;82:646–57.
27. Ni J, Chen C, Wang S, Liu X, Tan L, Lu L, Fan Y, Hou Y, Dou H, Liang J. Novel CSF biomarkers for diagnosis and integrated analysis of neuropsychiatric systemic lupus erythematosus: based on antibody profiling. *Arthritis Res Ther*. 2023;25:165.
28. Geng LY, Xu X, Zhang HY, Chen C, Hou YY, Yao GH, Wang SY, Wang DD, Feng XB, Sun LY, Liang J. Comprehensive expression profile of long non-coding RNAs in peripheral blood mononuclear cells from patients with neuropsychiatric systemic lupus erythematosus. *Annals Translational Med*. 2020;8.
29. Chen C, Geng L, Xu X, Kong W, Hou Y, Yao G, Feng X, Zhang H, Liang J. Comparative proteomics analysis of plasma protein in patients with neuropsychiatric systemic lupus erythematosus. *Ann Transl Med*. 2020;8:579.
30. Poggi L, Casarosa S, Carl M. An Eye on the wnt inhibitory factor Wif1. *Front Cell Dev Biol*. 2018;6:167.
31. Yu GD, Su YX, Guo C, Yi CJ, Yu B, Chen H, Cui YH, Wang XR, Wang YX, Chen XY, Wang SY, Wang Q, Chen XJ, Hu XL, Mei F, Verkhatsky A, Xiao L. Niu. Pathological oligodendrocyte precursor cells revealed in human schizophrenic brains and trigger schizophrenia-like behaviors and synaptic defects in genetic animal model. *Mol Psychiatr*. 2022;27:5154–66.
32. Chen W, Xia X, Song N, Wang Y, Zhu H, Deng W, Kong Q, Pan X, Qin C. Cross-species analysis of Gene expression and function in Prefrontal Cortex, Hippocampus and Striatum. *PLoS ONE*. 2016;11:e0164295.
33. Bis JC, DeCarli C, Smith AV, van der Lijn F, Crivello F, Fornage M, Debette S, Shulman JM, Schmidt H, Srikanth V, Schuur M, Yu L, Choi SH, Sigurdsson S, Verhaaren BF, DeStefano AL, Lambert JC, Jack CR Jr, Struchalin M, Stankovich J, Ibrahim-Verbaas CA, Fleischman D, Zijdenbos A, den Heijer T, Mazoyer B, Coker LH, Enzinger C, Danoy P, Amin N, Arfanakis K, van Buchem MA, de Bruijn RF, Beiser A, Dufouil C, Huang J, Cavalieri M, Thomson R, Niessen WJ, Chibnik LB, Gislason GK, Hofman A, Pkula A, Amouyel P, Freeman KB, Phan TG, Oostra BA, Stein JL, Medland SE, Vasquez AA, Hibar DP, Wright MJ, Franke B, Martin NG, Thompson PM, Meta-Analysis MA, Nalls AG, Uitterlinden R, Au A, Elbaz RJ, Beare JC, van Swieten OL, Lopez TB, Harris V, Chouraki MM, Breteler PL, De Jager JT, Becker MW, Vernooij D, Knopman P, Fazekas PA, Wolf A, van der Lugt V, Gudnason WT, Longstreth MA Jr, Brown DA, Bennett CM, van Duijn TH, Mosley R, Schmidt C, Tzourio LJ, Launer MA, Ikram S, Seshadri. Nat Genet. 2012;44:545–51. 12q24 are associated with hippocampal volume.
34. Humphries CE, Kohli MA, Nathanson A, Whitehead P, Beecham G, Martin E, Mash DC, Pericak-Vance MA. Gilbert. Integrated whole transcriptome and DNA methylation analysis identifies gene networks specific to late-onset Alzheimer's disease. *J Alzheimers Dis*. 2015;44:977–87.
35. Niu J, Tsai HH, Hoi KK, Huang N, Yu G, Kim K, Baranzini SE, Xiao L, Chan JR, Fancy SPJ. Aberrant oligodendroglial-vascular interactions disrupt the blood-brain barrier, triggering CNS inflammation. *Nat Neurosci*. 2019;22:709–18.
36. Lu C, Shao X, Zhou S, Pan C. LINC00176 facilitates CD4(+)T cell adhesion in systemic lupus erythematosus via the WNT5a signaling pathway by regulating WIF1. *Mol Immunol*. 2021;134:202–9.
37. Yokogawa M, Takaishi M, Nakajima K, Kamijima R, Fujimoto C, Kataoka S, Terada Y, Sano S. Epicutaneous application of toll-like receptor 7 agonists leads to systemic autoimmunity in wild-type mice: a new model of systemic lupus erythematosus. *Arthritis Rheumatol*. 2014;66:694–706.
38. Lu L, Liu X, Fu J, Liang J, Hou Y, Dou H. sTREM-1 promotes the phagocytic function of microglia to induce hippocampus damage via the PI3K-AKT signaling pathway. *Sci Rep*. 2022;12:7047.
39. Lu L, Wang H, Liu X, Tan L, Qiao X, Ni J, Sun Y, Liang J, Hou Y. Dou. Pyruvate kinase isoform M2 impairs cognition in systemic lupus erythematosus by promoting microglial synaptic pruning via the beta-catenin signaling pathway. *J Neuroinflammation*. 2021;18:229.
40. Tang XH, Zhang GF, Xu N, Duan GF, Jia M, Liu R, Zhou ZQ, Yang JJ. Extrasynaptic CaMKIIalpha is involved in the antidepressant effects of ketamine by downregulating GluN2B receptors in an LPS-induced depression model. *J Neuroinflammation*. 2020;17:181.
41. Bak J, Pyeon HI, Seok JI, Choi YS. Effect of rotation preference on spontaneous alternation behavior on Y maze and introduction of a new analytical method, entropy of spontaneous alternation. *Behav Brain Res*. 2017;320:219–24.

42. Song Y, Li X, Gong X, Zhao X, Ma Z, Xia T, Gu. Green tea polyphenols improve isoflurane-induced cognitive impairment via modulating oxidative stress. *J Nutr Biochem*. 2019;73:108213.
43. Dang RZ, Wang MY, Li XH, Wang HY, Liu LX, Wu QY, Zhao JT, Ji P, Zhong LM, Licinio J, Xie P. Edaravone ameliorates depressive and anxiety-like behaviors via Sirt1/Nrf2/HO-1/Gpx4 pathway. *J Neuroinflamm*. 2022;19.
44. Liu S, Fan M, Xu JX, Yang LJ, Qi CC, Xia QR, Ge JF. Exosomes derived from bone-marrow mesenchymal stem cells alleviate cognitive decline in AD-like mice by improving BDNF-related neuropathology. *J Neuroinflamm*. 2022;19.
45. Brueffer C, Saal LH. TopHat-Recondition: a post-processor for TopHat unmapped reads. *BMC Bioinformatics*. 2016;17.
46. Everaert C, Luybaert M, Maag JLV, Cheng QX, Dinger ME, Hellemans J. P. Mestdagh. Benchmarking of RNA-sequencing analysis workflows using wholetranscriptome RT-qPCR expression data. *Sci Rep-Uk*. 2017;7.
47. Qiao X, Wang H, Lu L, Chen J, Cheng Q, Guo M, Hou Y. Dou. Hippocampal microglia CD40 mediates NPSLE cognitive dysfunction in mice. *J Neuroimmunol*. 2021;357:577620.
48. Liu YS, Wang ML, Hu NY, Li ZM, Wu JL, Li H, Li JT, Li XW, Yang JM, Gao TM, Chen YH. A comparison of the impact on neuronal transcriptome and cognition of rAAV5 transduction with three different doses in the mouse hippocampus. *Front Mol Neurosci*. 2023;16:1195327.
49. Xu Y, Tang L, Zhou C, Sun L, Hu Y, Zhang Z, Xia S, Bao X, Yang H, Xu Y. Inhibition of ADORA3 promotes microglial phagocytosis and alleviates chronic ischemic white matter injury. *CNS Neurosci Ther*. 2024;30:e14742.
50. Phillips RG, LeDoux JE. Differential contribution of amygdala and hippocampus to cued and contextual fear conditioning. *Behav Neurosci*. 1992;106:274–85.
51. Sakic B, Szechtman H, Denburg JA. Neurobehavioral alterations in autoimmune mice. *Neurosci Biobehav R*. 1997;21:327–40.
52. Ballok DA, Szechtman H, Sakic B. Taste responsiveness and diet preference in autoimmune MRL mice. *Behav Brain Res*. 2003;140:119–30.
53. Sakic B, Denburg JA, Denburg SD, Szechtman. Blunted sensitivity to sucrose in autoimmune MRL-lpr mice: a curve-shift study. *Brain Res Bull*. 1996;41:305–11.
54. Sakic B, Szechtman H, Talangbayan H, Denburg SD, Carbotte RM, Denburg. Disturbed emotionality in Autoimmune Mrl-Lpr mice. *Physiol Behav*. 1994;56:609–17.
55. Sakic B, Szechtman H, Denburg S, Carbotte R, Denburg JA. Spatial-learning during the Course of Autoimmune-Disease in Mrl mice. *Behav Brain Res*. 1993;54:57–66.
56. Sakic B, Szechtman H, Keffer M, Talangbayan H, Stead R, Denburg JA. A behavioral Profile of Autoimmune Lupus-Prone Mrl mice. *Brain Behav Immun*. 1992;6:265–85.
57. Lisman J, Buzsaki G, Eichenbaum H, Nadel L, Ranganath C, Redish AD. Viewpoints: how the hippocampus contributes to memory, navigation and cognition. *Nat Neurosci*. 2017;20:1434–47.
58. Lalonde R. The neurobiological basis of spontaneous alternation. *Neurosci Biobehav R*. 2002;26:91–104.
59. Joëls M, Karst H, Sarabjitsingh RA. The stressed brain of humans and rodents. *Acta Physiol*. 2018;223.
60. Makinde HM, Winter DR, Procissi D, Mike EV, Stock AD, Kando MJ, Gadhi GT, Droho S, Bloomfield CL, Dominguez ST, Mayr MG, Lavine JA, Putterman C. C.M. Cuda. A novel microglia-specific transcriptional signature correlates with behavioral deficits in Neuropsychiatric Lupus. *Front Immunol*. 2020;11.
61. Ballok DA, Millward JM, Sakic B. Neurodegeneration in autoimmune MRL-lpr mice as revealed by Fluoro Jade B staining. *Brain Res*. 2003;964:200–10.
62. Hansen CE, Kamermans A, Mol K, Berve K, Rodriguez-Mogeda C, Fung WK, van het B, Hof RD, Fontijn SMA, van der Pol L, Michalick WM, Kuebler B, Kenkhuis W, van Roon-Mom W, Liedtke B, Engelhardt G, Kooij ME, Witte HE, De Vries. Inflammation-induced TRPV4 channels exacerbate blood-brain barrier dysfunction in multiple sclerosis. *J Neuroinflamm*. 2024;21.
63. Yun Y, Wang XJ, Xu JY, Chen JY, Wang XR, Yang PT, Qin L. Optogenetic stimulation of basal forebrain cholinergic neurons prevents neuroinflammation and neuropsychiatric manifestations in pristane induced lupus mice. *Behav Brain Funct*. 2023;19.
64. Carroll KR, Mizrachi M, Simmons S, Toz B, Kowal C, Wingard J, Tehrani N, Zarfeshani A, Kello N, El Khoury L, Weissman-Tsukamoto R, Levin JZ, Volpe BT, B. Diamond. Lupus autoantibodies initiate neuroinflammation sustained by continuous HMGB1:RAGE signaling and reversed by increased LAIR-1 expression. *Nat Immunol*. 2024.
65. Aw E, Zhang YY, Carroll M. Microglial responses to peripheral type 1 interferon. *J Neuroinflamm*. 2020;17.
66. Kerekes K, Trexler M, Bányai L. L. Pathy. Wnt inhibitory factor 1 binds to and inhibits the activity of Sonic hedgehog. *Cells*. 2021;10.
67. Alvarez JI, Dodelet-Devillers A, Kebir H, Ifergan I, Fabre PJ, Terouz S, Sabbagh M, Wosik K, Bourbonniere L, Bernard M, van Horsen J, de Vries HE, Charron F, Prat A. The hedgehog pathway promotes blood-brain barrier integrity and CNS immune quiescence. *Science*. 2011;334:1727–31.
68. Shao S, Wang GL, Raymond C, Deng XH, Zhu XL, Wang D, Hong LP. Activation of sonic hedgehog signal by Purmorphamine, in a mouse model of Parkinson's disease, protects dopaminergic neurons and attenuates inflammatory response by mediating PI3K/AKT signaling pathway. *Mol Med Rep*. 2017;16:1269–77.
69. Zhang H, Younsi A, Zheng G, Tail M, Harms AK, Roth J, Hatami M, Skutella T, Unterberg A. Zweckberger. Sonic hedgehog modulates the inflammatory response and improves functional recovery after spinal cord injury in a thoracic contusion-compression model. *Eur Spine J*. 2021;30:1509–20.
70. Kadry H, Noorani B, Cucullo L. A blood-brain barrier overview on structure, function, impairment, and biomarkers of integrity. *Fluids Barriers CNS*. 2020;17:69.
71. Qiu J, Yan Z, Tao K, Li Y, Li J, Dong Y, Feng D. Chen. Sinomenine activates astrocytic dopamine D2 receptors and alleviates neuroinflammatory injury via the CRYAB/STAT3 pathway after ischemic stroke in mice. *J Neuroinflammation*. 2016;13:263.
72. Huang R, Zhang C, Zheng Y, Zhang W, Huang H, Qiu M, Li J, Li F. ISL1 regulates lung branching morphogenesis via shh signaling pathway. *J Biol Chem*. 2023;299:105034.
73. Wang Y, Ali M, Zhang Q, Sun Q, Ren J, Wang W, Tang D, Wang D. ATF4 transcriptionally activates SHH to promote proliferation, Invasion, and Migration of Gastric Cancer cells. *Cancers (Basel)*. 2023;15.
74. Wang Y, Wu M, Chen D, Tan B, Lin P, Huang D, Ye C. SDMA attenuates renal tubulointerstitial fibrosis through inhibition of STAT4. *J Transl Med*. 2023;21:326.
75. Rayes HA, Tani C, Kwan A, Marzouk S, Colosimo K, Medina-Rosas J, Mustafa A, Su J, Lambiris P, Mosca M, Touma. What is the prevalence of cognitive impairment in lupus and which instruments are used to measure it? A systematic review and meta-analysis. *Semin Arthritis Rheum*. 2018;48:240–55.
76. Rassnick S, Zhou D, Rabin BS. Central administration of prostaglandin E2 suppresses in vitro cellular immune responses. *Am J Physiol*. 1995;269:R92–97.
77. Sakić B, Szechtman H, Talangbayan H, Denburg S, Carbotte R, Denburg JA. Behavior and immune status of MRL mice in the postweaning period. *Brain Behav Immun*. 1994;8:1–13.
78. Yu G, Su Y, Guo C, Yi C, Yu B, Chen H, Cui Y, Wang X, Wang Y, Chen X, Wang S, Wang Q, Chen X, Hu X, Mei F, Verkhatsky A, Xiao L, Niu J. Pathological oligodendrocyte precursor cells revealed in human schizophrenic brains and trigger schizophrenia-like behaviors and synaptic defects in genetic animal model. *Mol Psychiatry*. 2022;27:5154–66.
79. Suresh S, Vellapandian C. Cyanidin ameliorates Bisphenol A-Induced Alzheimer's Disease Pathology by restoring Wnt/ β -Catenin Signaling Cascade: an in Vitro Study. *Mol Neurobiol*. 2024;61:2064–80.
80. Seet D, Allameen NA, Tay SH, Cho J, Mak A. Cognitive dysfunction in systemic Lupus Erythematosus: Immunopathology, Clinical manifestations, neuroimaging and Management. *Rheumatol Ther*. 2021;8:651–79.
81. Muraleva NA, Kolosova NG, Stefanova. p38 MAPK-dependent alphas-crystallin phosphorylation in Alzheimer's disease-like pathology in OXYS rats. *Exp Gerontol*. 2019;119:45–52.
82. Liu Y, Zhou Q, Tang M, Fu N, Shao W, Zhang S, Yin Y, Zeng R, Wang X, Hu G. Zhou. Upregulation of alphas-crystallin expression in the substantia nigra of patients with Parkinson's disease. *Neurobiol Aging*. 2015;36:1686–91.
83. Lim EF, Hoghooghi V, Hagen KM, Kapoor K, Frederick A, Finlay TM, Ousman SS. Presence and activation of pro-inflammatory macrophages are associated with CRYAB expression in vitro and after peripheral nerve injury. *J Neuroinflammation*. 2021;18:82.
84. Becerra-Hernandez LV, Escobar-Betancourt MI, Pimienta-Jimenez HJ. Buritica. Crystallin Alpha-B overexpression as a possible marker of reactive astrogliosis in human cerebral contusions. *Front Cell Neurosci*. 2022;16:838551.
85. Ren Z, Yang M, Guan Z. Yu. Astrocytic $\alpha 7$ nicotinic receptor activation inhibits Amyloid- β aggregation by upregulating endogenous $\alpha 8$ -crystallin through the PI3K/Akt signaling pathway. *Curr Alzheimer Res*. 2019;16:39–48.
86. Zeis T, Graumann U, Reynolds R, Schaeren-Wiemers N. Normal-appearing white matter in multiple sclerosis is in a subtle balance between inflammation and neuroprotection. *Brain*. 2008;131:288–303.

87. Jee Y, Kim G, Tanuma N, Matsumoto Y. STAT expression and localization in the central nervous system during autoimmune encephalomyelitis in Lewis rats. *J Neuroimmunol.* 2001;114:40–7.
88. Zhang X, Wang Y, Lv J. STAT4 targets KISS1 to inhibit the oxidative damage, inflammation and neuronal apoptosis in experimental PD models by inactivating the MAPK pathway. *Neurochem Int.* 2024;175:105683.
89. Li X, Li Y, Li S, Li H, Yang C, Lin J. The role of shh signalling pathway in central nervous system development and related diseases. *Cell Biochem Funct.* 2021;39:180–9.
90. Abbott NJ, Ronnback L, Hansson E. Astrocyte-endothelial interactions at the blood-brain barrier. *Nat Rev Neurosci.* 2006;7:41–53.
91. Sen P, Roy Acharyya S, Arora A, Ghosh SS. An in-silico approach to understand the potential role of wnt inhibitory factor-1 (WIF-1) in the inhibition of the wnt signalling pathway. *J Biomol Struct Dyn.* 2024;42:326–45.
92. Chen S, Li N, Deb-Chatterji M, Dong Q, Kielstein JT, Weissenborn K, Worthmann. Asymmetric dimethylarginine as marker and mediator in ischemic stroke. *Int J Mol Sci.* 2012;13:15983–6004.
93. Schwedhelm E, Böger RH. The role of asymmetric and symmetric dimethylarginines in renal disease. *Nat Rev Nephrol.* 2011;7:275–85.
94. Fleszar MG, Wiśniewski J, Zboch M, Diakowska D, Gamin A, Krzystek-Korpacka M. Targeted metabolomic analysis of nitric oxide/L-arginine pathway metabolites in dementia: association with pathology, severity, and structural brain changes. *Sci Rep.* 2019;9:13764.
95. Cieślak P, Siekierzycka A, Radulska A, Płoska A, Burnat G, Brański P, Kalinowski L, J.M. Wierońska. Nitric oxide-dependent mechanisms underlying MK-801- or Scopolamine-Induced memory dysfunction in animals: mechanistic studies. *Int J Mol Sci.* 2021;22.

Publisher's note

Springer Nature remains neutral with regard to jurisdictional claims in published maps and institutional affiliations.